

The Power of Decaying Steps: Enhancing Attack Stability and Transferability for Sign-based Optimizers

Wei Tao^{1,2,†}, Yang Dai^{1,†}, Jincui Huang¹, Qing Tao^{3,*}

¹ Laboratory for Big Data and Decision, National University of Defense and Technology, China

² Academy of Military Science, China

³ Hefei Institute of Technology, China

Abstract

Crafting adversarial examples can be formulated as an optimization problem. While sign-based optimizers such as I-FGSM and MI-FGSM have become the de facto standard for the induced optimization problems, there still exist several unsolved problems in theoretical grounding and practical reliability especially in non-convergence and instability, which inevitably influences their transferability. Contrary to the expectation, we observe that the attack success rate may degrade sharply when more number of iterations are conducted. In this paper, we address these issues from an optimization perspective. By reformulating the sign-based optimizer as a specific coordinate-wise gradient descent, we argue that one cause for non-convergence and instability is their non-decaying step-size scheduling. Based upon this viewpoint, we propose a series of new attack algorithms that enforce Monotonically Decreasing Coordinate-wise Step-sizes (MDCS) within sign-based optimizers. Typically, we further provide theoretical guarantees proving that MDCS-MI attains an optimal convergence rate of $O(1/\sqrt{T})$, where T is the number of iterations. Extensive experiments on image classification and cross-modal retrieval tasks demonstrate that our approach not only significantly improves transferability but also enhances attack stability compared to state-of-the-art sign-based methods.

1. Introduction

Crafting adversarial examples (AEs) for a given learning model can be cast as a constrained local optimization problem [13]. The defining objective is to seek an imperceptible perturbation to the input data that induces a maximal loss in the model’s output. In the landscape of attack methodologies, sign-based gradient optimizers have long been the dominant paradigm. This family of algorithms includes the foundational single-step FGSM [13], its multi-step refine-

ments I-FGSM (BIM) [21] and PGD [27], as well as the momentum-enhanced MI-FGSM [7].

FGSM and I-FGSM are directly developed from the well-known gradient descent principle, in which the sign of the gradient vector is used as its update direction. Similar to sign-gradient, MI-FGSM [7] uses the sign of a variant of Polyak’s heavy-ball (HB) momentum [29] as its iterative direction. By accumulating the past gradients in momentum, MI-FGSM can stabilize update directions and then remarkably boost the transferability of AEs.

MI-FGSM has won the first place in NIPS 2017 Non-targeted Adversarial Attack and Targeted Adversarial Attack competitions [7]. To further enhance transferability, various sign-based momentum attacks have been proposed by incorporating insight from optimization theory. Typical examples include VMI-FGSM [39], GRA [50], PGN [12], MEF [30], and MUMIDIG [32]. Concurrently, recent studies have exposed that Vision-Language Models (VLMs) remain vulnerable to AEs [5, 46]. A key distinction in this multimodal setting is the necessity for collaborative perturbation across modalities, rather than independent attacks. Pioneering this direction, Co-Attack [46] collectively generate adversarial perturbations for both image and text modalities. Subsequent methods like SGA, DRA, and SA-AET [11, 17, 26] have further pushed the state-of-the-art by augmenting image-text pairs. Notably, despite the progressive complexity in their multimodal attack strategies, these methods share a common algorithmic backbone, i.e., they fundamentally rely on sign-based optimizers as the core engine for perturbation generation.

Despite the demonstrated transferability of sign-based optimizers, there still exist several unsolved problems in theoretical grounding and practical reliability. Theoretically, the convergence guarantees of these methods are fundamentally flawed. As established by Karimireddy et al. [19], even in simple convex settings which are a canonical test bed for optimization, sign-based gradients provably fail to converge to optimum. This divergence is intrinsic to the sign operator. It only acts as an extreme form of compress-

[†]equal contribution, ^{*} corresponding author

sion, discarding crucial information about gradient magnitudes and distorting the true descent direction.

The theoretical fragility manifests in practice as a counter-intuitive operational instability. Contrary to the expectation that conducting more iterations would enhance an attack, we observe an obvious degradation in success rates under prolonged optimization. As quantified in Fig. 1, the performance of I-FGSM and MI-FGSM deteriorates when more number of iterations are conducted. Notably, the success rate of I-FGSM plummets from a peak of 37.1% ($t = 2$) to a trough of 15.5% ($t = 20$). This performance collapse indicates that the sign-based optimizers are prone to overshooting or oscillating around the optimal attack rate, thereby highlighting a critical limitation in their operational stability and reliability.

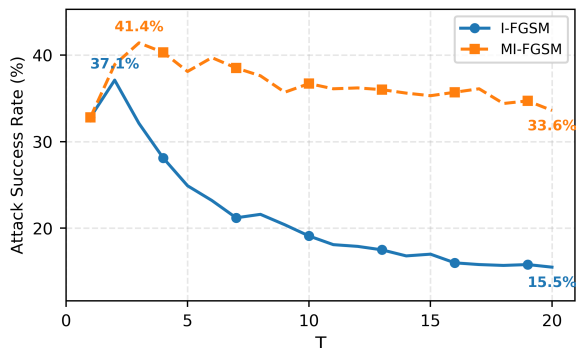


Figure 1. Stability comparison of typical sign-based transfer attacks on the NIPS2017 dataset. We employ Res50 as surrogate model and Inc-v3 as target model with $\epsilon = 16/255$.

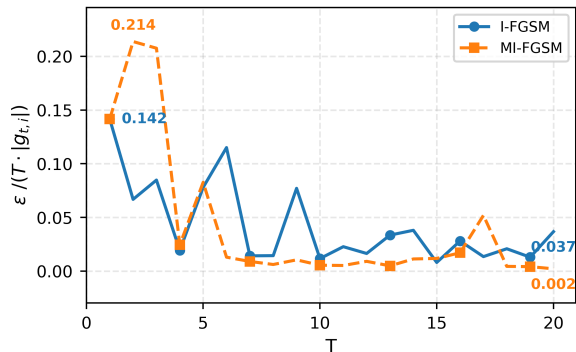


Figure 2. Step-size dynamics of a randomly selected coordinate in typical sign-based attacks. T is the maximum iteration. We reformulate $\text{sign}(\mathbf{g}_t)$ as $\mathbf{g}_{t,i}/|\mathbf{g}_{t,i}|$ where \mathbf{g} denotes the gradient or momentum and i is the number of the randomly selected coordinate. So, the step-size is $\epsilon/(T|\mathbf{g}_{t,i}|)$ for coordinate-wise gradient.

To discuss the convergence failures of sign-based gradient, we are naturally led to investigate their step-size scheduling. With regard to the sign-based gradient direc-

tion, the step-size is usually set to constant such as $\alpha = \epsilon/T$, where T is the total number of iterations. However, when reformulating I-FGSM as a standard coordinate-wise gradient descent, we reveal that the step-size for each coordinate becomes heavily depends on its gradient magnitude, thereby violating the classical conditions for convergence that require step-size decaying. As visualized in Fig. 2, we plot the progression of a randomly chosen coordinate, the step-sizes in I-FGSM fluctuate without any discernible decaying structure. While the momentum can avoid the fluctuation of an individual gradient, this non-decreasing behavior is similarly pronounced in MI-FGSM, confirming that non-decaying step-size scheduling is an inherent characteristic of sign-based optimization paradigms.

In iterative optimization, a large initial step-size often facilitates rapid progress toward a region near the optimum, whereas a subsequent gradual decay enables finer adjustments for stable convergence. This behavior is particularly important in adversarial attacks, where only a limited number of iterations is performed for the constrained local optimization. It should be indicated that the strategy of using a monotonically decreasing step-size occupies a central position in optimization theory, serving as a foundational component for algorithm design with both theoretical and practical importance. It provides essential convergence guarantees for a broad family of iterative methods. For example, in the convex setting, classical schedules such as $\alpha_t = \alpha/\sqrt{t}$ ensure that the regular gradient descent method achieves an optimal convergence rate of $O(1/\sqrt{t})$ [6].

A seminal adaptation of monotonically decreasing step-size to the coordinate-wise setting is the work of the adaptive mechanism known as AdaGrad [10]. Unlike global decaying schedules, AdaGrad adapts each coordinate-wise step-size inversely to the root sum of squares of its past gradients. This construction naturally enforces a monotonically decreasing coordinate-wise step-size (MDCS), allowing AdaGrad to achieve a tighter optimal convergence rate for general convex objectives in sparse learning.

The critical importance of MDCS was underscored by the failure of convergence analysis about Adam [20] identified in [31]. Their analysis shows that enforcing MDCS rectifies this issue, leading to the development of AMSGrad. Although Adam has long been the dominant optimizer for training deep neural networks, AMSGrad, despite being a simple variant by incorporating MDCS, not only easily derives theoretical convergence but also frequently outperforms Adam in empirical evaluations [31].

The frequent fluctuation of the sign of perturbation has already been observed in [50]. Such fluctuations can cause the optimization to stagnate in local optima due to the constant step-size used in sign-based optimizers. To mitigate this issue, they introduced a decay indicator that dynamically adjusts the step-size in response to sign fluctuations,

thereby enhancing the overall optimization process [50].

Building upon the aforementioned analysis, we will incorporate MDCS into state-of-the-art sign-based optimizers to address their non-convergence and instability issues. Our contributions can be summarized as follows,

- By reformulating sign-based optimizer as a specific coordinate-wise gradient descent, we present an interesting viewpoint from the perspective of optimization, revealing that one cause for the attack instability is their step-size rule.
- Based on our new viewpoint, we propose a series of new attack algorithms to enhance stability, in which MDCS is enforced in sign-based optimizers. Typically, we prove that MI-FGSM with MDCS attains its optimal averaging convergence for general convex problems.
- Experimental comparisons with state-of-the-art sign-based optimizers on image classification, VQA and image-text retrieval tasks illustrate that our approach not only significantly improves the attack success rates but also enhances their stability.

2. Related Work

In this section, we describe the optimization problem for adversarial attacks and several typical optimizers.

Let $\mathcal{S} = \{(\mathbf{x}_1, y_1), \dots, (\mathbf{x}_m, y_m)\}$ be a training set, where y_i is the label of $\mathbf{x}_i \in \mathbb{R}^d$. Given a classifier f_θ with a predefined θ , generating a non-targeted AE \mathbf{x}^{adv} from a real example \mathbf{x} can be formulated as a constrained optimization problem [13, 27],

$$\max J(f_\theta(\mathbf{x}^{adv}), y), \text{ s.t. } \|\mathbf{x}^{adv} - \mathbf{x}\|_p \leq \epsilon, \quad (1)$$

where $J(f_\theta(\mathbf{x}), y)$ is the loss function. Obviously, optimization problem (1) coincides with our intuition, i.e., adversarial attack is to find an AE that misleads the model prediction (i.e., $f_\theta(\mathbf{x}^{adv}) \neq y$) while the L_p -norm of the adversarial perturbation $\|\mathbf{x}^{adv} - \mathbf{x}\|_p$ should be restricted to a threshold ϵ . As the constrained domain is typically small under the imperceptibility constraint, problem (1) becomes a local optimization problem, which is a key distinction from conventional optimization settings. In this paper, we only consider the cross-entropy loss and $p = \infty$. For convenience, we denote $\mathbf{Q} = \{\mathbf{z} : \|\mathbf{z} - \mathbf{x}\|_\infty \leq \epsilon\}$ and rewrite $J(f_\theta(\mathbf{x}^{adv}), y)$ as $J(\mathbf{x}^{adv})$.

FGSM [13] is a basic gradient-based attack. It has only one-step update, i.e.,

$$\mathbf{x}^{adv} = \mathbf{x} + \epsilon \text{sign}(\nabla_{\mathbf{x}} J(\mathbf{x})), \quad (2)$$

where $\text{sign}(\cdot)$ is the sign function. From (2), it is easy to know $\|\mathbf{x}^{adv} - \mathbf{x}\|_\infty \leq \epsilon$.

I-FGSM [21] is a FGSM with multiple iterative steps,

$$\mathbf{x}_{t+1}^{adv} = \mathbf{x}_t^{adv} + \alpha \text{sign}(\nabla_{\mathbf{x}} J(\mathbf{x}_t^{adv})), \quad (3)$$

where $\mathbf{x}_0^{adv} = \mathbf{x}$. The step-size α is set to ϵ/T so that $\|\mathbf{x}_t^{adv} - \mathbf{x}\|_\infty \leq \epsilon$, $0 \leq \forall t \leq T$, where T is the total number of iterations. It should be noted that α only determines the magnitude of the update along $\text{sign}(\nabla_{\mathbf{x}} J(\mathbf{x}_t^{adv}))$ rather than along its real gradient $\nabla_{\mathbf{x}} J(\mathbf{x}_t^{adv})$.

PGD [27] is also multiple iterative steps FGSM but starting from a random starting point, i.e.,

$$\mathbf{x}_{t+1}^{adv} = \text{Clip}_{\mathbf{x}}^\epsilon [\mathbf{x}_t^{adv} + \alpha \text{sign}(\nabla_{\mathbf{x}} J(\mathbf{x}_t^{adv}))], \quad (4)$$

As the step-size is not restricted, a clipping (5) operation is used to ensure that $\|\mathbf{x}^{adv} - \mathbf{x}\|_\infty \leq \epsilon$. For an image $\mathbf{x} = (x_1, x_2, x_3)$ which is 3-D tensor, its clipping is [21]

$$\text{Clip}_{\mathbf{x}}^\epsilon [\mathbf{x}(x_1, x_2, x_3)] = \min\{255, \mathbf{x}(x_1, x_2, x_3) + \epsilon, \max\{0, \mathbf{x}(x_1, x_2, x_3) - \epsilon, \mathbf{x}(x_1, x_2, x_3)\}\}. \quad (5)$$

MI-FGSM [7] integrates HB momentum [29] into the iteration of I-FGSM. Its update is

$$\begin{aligned} \mathbf{m}_{t+1} &= \mu \mathbf{m}_t + \frac{\nabla_{\mathbf{x}} J(\mathbf{x}_t^{adv})}{\|\nabla_{\mathbf{x}} J(\mathbf{x}_t^{adv})\|_1}, \\ \mathbf{x}_{t+1}^{adv} &= \text{Clip}_{\mathbf{x}}^\epsilon (\mathbf{x}_t^{adv} + \alpha \text{sign}(\mathbf{m}_{t+1})) \end{aligned} \quad (6)$$

where $\alpha = \epsilon/T$. Note that \mathbf{m}_{t+1} is the sum of weighted past gradients and then this iterative direction is more stable than the individual $\text{sign}(\nabla_{\mathbf{x}} J(\mathbf{x}_t^{adv}))$ in I-FGSM and PGD.

Based upon MI-FGSM, a number of momentum-based attack methods have been developed by employing more techniques from optimization theory. For instance, NI-FGSM [23] integrates Nesterov's momentum, VMI-FGSM [39] introduces variance tuning, and GRA [50] incorporates variance tuning and decay indicator techniques. Recent studies suggest that AEs located at flat maxima of the loss landscape tend to exhibit stronger transferability. For example, PGN [12] and MEF [30] mitigate this issue by incorporating a gradient norm penalty into the loss.

Another line of work focuses on improving transferability through input transformation. DI [42] pioneered this direction by applying random resizing and padding to inputs. This was followed by techniques such as TI [8], SI [23], Admix [38], and BSR [37]. Such transformation strategies are commonly integrated with optimization-based attacks. Recently, OPS [14] improves optimization efficiency by randomly selecting transformations at each iteration, thereby promoting gradient diversity during the attack process.

Recent efforts to generate transferable AEs for VLMs have progressively focused on enhancing sample diversity. Initial works like Co-Attack [46] established a baseline with collaborative multimodal perturbations. Subsequently, SGA [26] employed online data augmentation, which was refined by DRA [11] through sampling within the adversarial trajectory's intersection to mitigate overfitting. SA-AET [17] further leverage an adversarial evolution triangle for

more principled diversification while simultaneously crafting attacks in a semantic-aligned subspace to reduce model dependency. Despite the increasing sophistication in handling multimodal interactions, all these methods retain PGD as their underlying optimizer to generate AEs.

3. The Proposed MDCS

In this section, we first reformulate I-FGSM as a coordinate-wise gradient descent and explicitly describe its step-size scheme, then we propose our MDCS strategy.

Let $x_{t+1,i}^{adv}$ be the i -th component of \mathbf{x}_{t+1}^{adv} generated by I-FGSM, i.e.,

$$x_{t+1,i}^{adv} = x_{t,i}^{adv} + \alpha \operatorname{sign}\left(\frac{\partial J(\mathbf{x}_t^{adv})}{\partial x_i}\right).$$

Then, we have

$$x_{t+1,i}^{adv} = x_{t,i}^{adv} + \frac{\alpha}{\left|\frac{\partial J(\mathbf{x}_t^{adv})}{\partial x_i}\right|} \frac{\partial J(\mathbf{x}_t^{adv})}{\partial x_i}. \quad (7)$$

According to optimization theory, the coordinate-wise step-size in I-FGSM is formally defined as $\frac{\alpha}{\left|\frac{\partial J(\mathbf{x}_t^{adv})}{\partial x_i}\right|}$. This formulation implies that the step-size is governed by the gradient magnitude. As the attack converges near a local optimum, the gradient approaches zero, causing the step-size to diverge and exhibit unexpected fluctuations, a behavior we depict in Fig. 2.

The step-size analysis for I-FGSM is fully applicable to all the sign-based optimizers. Specifically, the coordinate-wise step-size of MI-FGSM is $\frac{\alpha}{|m_{t+1,i}|}$. The key distinction lies in the fact that MI-FGSM enjoys better stability owing to momentum being a weighted sum of past gradients.

Note that the regular Adam [20] for solving problem (1) is

$$\begin{aligned} \mathbf{m}_t &= \beta_{1t} \mathbf{m}_{t-1} + (1 - \beta_{1t}) \nabla_{\mathbf{x}} J(\mathbf{x}_t), \\ \mathbf{V}_t &= \beta_{2t} \mathbf{V}_{t-1} + (1 - \beta_{2t}) \operatorname{diag}(\nabla_{\mathbf{x}} J(\mathbf{x}_t) \nabla_{\mathbf{x}} J(\mathbf{x}_t)^\top), \\ \mathbf{x}_{t+1} &= P_{\mathbf{Q}, \mathbf{V}_t^{-1}}(\mathbf{x}_t - \alpha_t \mathbf{V}_t^{-\frac{1}{2}} \mathbf{m}_t), \end{aligned} \quad (8)$$

where the hyper-parameters $\beta_{1t}, \beta_{2t} \in [0, 1)$ control the exponential decay rates of the moving averages (EMA), and \mathbf{V}_t is a $d \times d$ diagonal matrix. For a positive definite matrix \mathbf{V}_t^{-1} , the weighted L_2 -norm (Mahalanobis norm) is defined by $\|\mathbf{x}\|_{\mathbf{V}_t^{-1}}^2 = \mathbf{x}^\top \mathbf{V}_t^{-1} \mathbf{x}$. The projection $P_{\mathbf{Q}, \mathbf{V}_t^{-1}}(\mathbf{x})$ of \mathbf{x} onto \mathbf{Q} is defined by

$$P_{\mathbf{Q}, \mathbf{V}_t^{-1}}(\mathbf{x}) = \min_{\mathbf{z} \in \mathbf{Q}} \|\mathbf{x} - \mathbf{z}\|_{\mathbf{V}_t^{-1}} = \min_{\mathbf{z} \in \mathbf{Q}} \|\mathbf{V}_t^{-\frac{1}{2}}(\mathbf{x} - \mathbf{z})\|.$$

The primary challenge in establishing the convergence guarantee for Adam-type optimizers [20] stems from their use of EMA, which can violate the standard step-size decay condition required for conventional theoretical analysis

[31]. To resolve this theoretical issue, Reddi et al. [31] demonstrate that provable convergence can be readily recovered by enforcing MDCS, i.e.,

$$\begin{aligned} \mathbf{m}_t &= \beta_{1t} \mathbf{m}_{t-1} + (1 - \beta_{1t}) \nabla_{\mathbf{x}} J(\mathbf{x}_t), \\ \mathbf{V}_t &= \beta_{2t} \mathbf{V}_{t-1} + (1 - \beta_{2t}) \operatorname{diag}(\nabla_{\mathbf{x}} J(\mathbf{x}_t) \nabla_{\mathbf{x}} J(\mathbf{x}_t)^\top), \\ \hat{\mathbf{V}}_t &= \max\{\hat{\mathbf{V}}_{t-1}, \mathbf{V}_t\} \\ \mathbf{x}_{t+1} &= P_{\mathbf{Q}, \hat{\mathbf{V}}_t^{-1}}(\mathbf{x}_t - \alpha_t \hat{\mathbf{V}}_t^{-\frac{1}{2}} \mathbf{m}_t). \end{aligned} \quad (9)$$

Such an algorithm is called AMSGrad [31]. It has been proved to attain the optimal convergence while deriving better empirical performance in image classification [31].

Motivated by AMSGrad, we propose a broad class of optimizers based on available sign-based attacks, which ensures that the coordinate-wise step-size is monotonically decreasing. Specifically, the detailed steps of MI-FGSM with MDCS are shown in Algorithm 1.

Algorithm 1 MDCS-MI

Input: Loss function J , a raw example \mathbf{x} with ground-truth label y , the perturbation size ϵ , momentum parameter $0 < \beta_t \leq 1$, step-size $\alpha_t > 0$, maximum iteration T .

1: Initialize $\mathbf{x}_0^{adv} = \mathbf{x}$, $\mathbf{m}_1 = \mathbf{0}$, $d_{0,i} = 1$.

2: **repeat**

3: $\mathbf{m}_{t+1} = \beta_t \mathbf{m}_t + \frac{\nabla_{\mathbf{x}} J(\mathbf{x}_t^{adv})}{\|\nabla_{\mathbf{x}} J(\mathbf{x}_t^{adv})\|_1}$,

4: $d_{t,i} = \min\left(\frac{1}{|m_{t+1,i}|}, d_{t-1,i}\right)$,

5: $\mathbf{D}_t = \operatorname{diag}(\mathbf{d}_t)$,

6: $\mathbf{x}_{t+1}^{adv} = P_{\mathbf{Q}, \mathbf{D}_t^{-1}}(\mathbf{x}_t^{adv} + \alpha_t \mathbf{D}_t \mathbf{m}_{t+1})$.

7: **until** $t = T$

Output: \mathbf{x}_T^{adv} .

For an image $\mathbf{x} = (x_1, x_2, x_3)$ which is 3-D tensor,

$$\begin{aligned} \mathbf{x}_{t+1}^{adv} &= P_{\mathbf{Q}, \mathbf{D}_t^{-1}}(\mathbf{x}_t^{adv} + \alpha_t \mathbf{D}_t \mathbf{m}_{t+1}) \\ &= \operatorname{Clip}_{\mathbf{x}}^\epsilon \left[\mathbf{D}_t^{-\frac{1}{2}} (\mathbf{x}_t^{adv} + \alpha_t \mathbf{D}_t \mathbf{m}_{t+1}) \right]. \end{aligned} \quad (10)$$

It is easy to find that $d_{t,i} \leq d_{t-1,i} \leq 1, \forall t > 0$. Obviously, the main difference from MI-FGSM is that we employ MDCS instead of the sign operation. To conduct convergence analysis, some assumptions are required. The detailed proof is given in Supplementary Material.

Assumption 1. Assume that there exists a constant $M > 0$ such that

$$\|\nabla_{\mathbf{x}} J(\mathbf{x})\|_1 \leq M, \forall \mathbf{x} \in \mathbf{Q}.$$

Assumption 2. Assume that there exists a constant $G > 0$ such that

$$\|\mathbf{x}_1 - \mathbf{x}_2\| \leq G, \forall \mathbf{x}_1, \mathbf{x}_2 \in \mathbf{Q}.$$

Theorem 3. Suppose the objective function $J(\mathbf{x})$ is concave on \mathbf{Q} and \mathbf{x}^* is a solution of problem (1). Let Assumption 1 and 2 hold and let $\{\mathbf{x}_t^{adv}\}_{t=1}^T$ be generated by Algorithm 1. Assume $0 < \beta < 1$, $0 < \lambda < 1$ and $\gamma > 0$. Let $\beta_t = \beta\lambda^{t-1}$ and $\alpha_t = \frac{\gamma}{\sqrt{t}}$. Then we have

$$J(\mathbf{x}^*) - J(\bar{\mathbf{x}}_T^{adv}) \leq O\left(\frac{1}{\sqrt{T}}\right)$$

where $\bar{\mathbf{x}}_T^{adv} = \frac{1}{T} \sum_{t=1}^T \mathbf{x}_t^{adv}$.

It is necessary to give some remarks.

- Theorem 3 indicates that MDCS-MI achieves optimal convergence rate $O(1/\sqrt{T})$, which avoids the non-convergence issue inherent in MI-FGSM caused by the sign-based operation.
- Our theoretical analysis can be readily extended to other sign-based optimizers such as I-FGSM and PGD. Due to using MDCS, the proof here is similar to that of AdaGrad and AMSGrad in spirit.
- If an AE \mathbf{x}^{adv} is successfully generated from a correctly classified sample \mathbf{x} , it holds that $J(\mathbf{x}^{adv}) > J(\mathbf{x})$. The human-imperceptibility constraint restricts \mathbf{x}^{adv} to a confined neighborhood of \mathbf{x} , thus justifying the mild assumption that the objective function is locally concave.

4. Experiments

In this section, we show the efficacy of our MDCS strategy through extensive experiments on image classification models and VLMs. Typically, we only focus on comparing with some recent optimization-based methods under untargeted attack setting, using their standard hyperparameters. Transferability is quantified by the attack success rate, with a higher rate denoting more effective and transferable attacks. All experiments were performed on Hygon K100-AI 64GB DCUs. Due to the space limitation, more details and experimental results are given in **Supplementary Material**.

4.1. Evaluation on Image Classification Tasks

Since our MDCS-MI is directly established upon MI-FGSM, we will conduct the same experiments as that in [7]. Following [7] and [23], we randomly sample 1000 images from NIPS2017 dataset. The normally trained models are chosen from both branches of CNNs and ViTs for black-box attacks, including ResNet-50 (Res50), VGG-16, MobileNet-v2 (Mob-v2), Inception-v3 (Inc-v3) in CNN branch; ViT-Base-patch16 (ViT-B/16) [9], PiT-Base (PiT-B) [15], Visformer-Small (Vis-S) [3] in ViT branch. Following [22], we also collect robust Inc-v3_{ens3}, Inc-v3_{ens4}, IncRes-v2_{ens} and consider AT, HGD, RS, Bit-Red as defended models.

The hyperparameters in problem (1) are fixed. We set $\epsilon = 16/255$ and $T = 10$. As usual, $\lambda = 0.999$ and $\beta =$

0.999 [31, 35, 36]. For convenience, we select $\alpha_t = \epsilon\gamma/T$ in our MDCS-type algorithms. γ is determined by simple grid search over the range [2, 4] to balance transferability and imperceptibility.

4.1.1. Evaluation of Attack Stability

To illustrate the benefits brought by our MDCS strategy, we examine the correlation between success rates and the maximum iteration T . As depicted in Fig. 3, integrating HB momentum into the iterative direction in MI-FGSM does contribute to stability. Nonetheless, MDCS can improve transferability of MI-FGSM across different neural network architectures while consistently maintaining better stability.

4.1.2. Attacks on Normally Trained Models

In this subsection, we evaluate the adversarial transferability of the proposed attack on normally trained models including both single and ensemble architectures. As far as we know, OPS [14] currently achieves highly competitive performance compared to typical baseline attacks such as MI-FGSM [7], VMI-FGSM [39], PGN [12] and MEF [30]. Based on these findings and considering the central role of OPS as a state-of-the-art approach, we focused our subsequent comparative experiments primarily on MI-FGSM, MEF and OPS. In addition to single-model attacks, we evaluate our MDCS strategy in ensemble-model settings. Specifically, we focus on attacking an ensemble of equally-weighted models using logit-based integration. For comparative baselines, we include SVRE [43] and AdaEA [1].

As shown in Tab. 1 and 2, MDCS-MI consistently surpasses MI-FGSM in both single-model and ensemble attacks. Moreover, integrating MDCS into other attacks also improves their transferability, with MDCS-OPS achieving the best performance. Visualizations in Fig. 5 confirm that the adversarial perturbations generated by our methods (MDCS-MI, MDCS-MEF, MDCS-OPS) remain imperceptible, thereby satisfying the requirement for stealth in practical scenarios.

4.1.3. Attacks on Robust Models

In this subsection, we evaluate the performance of the crafted AEs in defense and adversarial training scenarios. For simplicity, AEs are crafted for Res50. The success rates are reported in Tab. 3. It can be observed that the success rates of typical adversarial attacks exhibit varying degrees of improvement after incorporating our MDCS strategy. Specifically, MDCS-OPS achieves the best results, which validate the effectiveness of the proposed MDCS strategy in defense scenarios.

4.1.4. Ablation Study

While both ϵ and γ in MDCS-MI critically affect the performance, we focus here on ablating the perturbation budget ϵ . A detailed analysis of γ is deferred to Sec. 8.1.2.

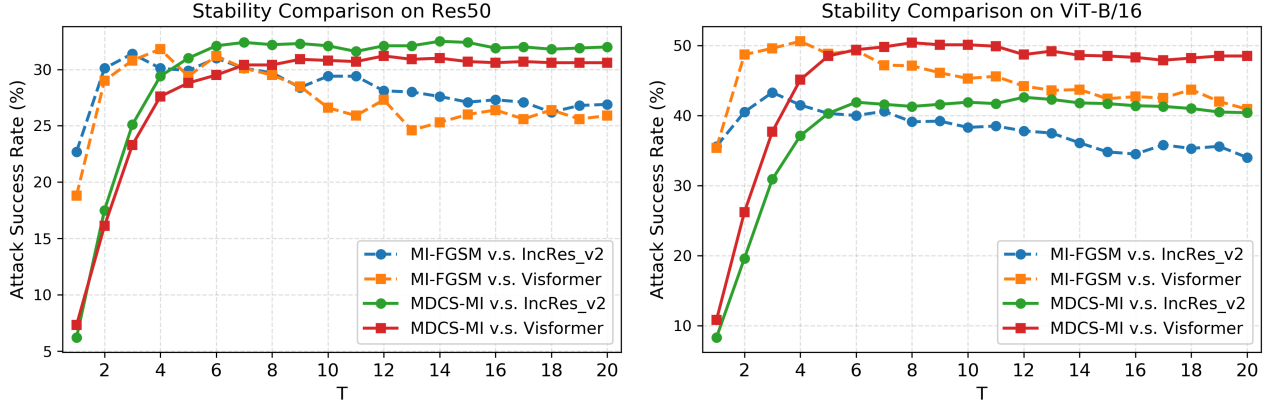


Figure 3. Stability comparison of transfer attacks between MDCS-MI and MI-FGSM. AEs are crafted for Res50 and ViT-B/16, respectively.

Table 1. Transferability comparisons across different network architectures. AEs are crafted for Res50. The baseline attacks are divided into 3 categories: ① gradient-based attacks; ② momentum-based attacks; ③ input-transformation attacks. The best results are marked in bold. The gray area represents adversarial attacks under the white-box setting.

| Type | Attack | Res50 | VGG16 | Mob-v2 | Inc-v3 | ViT-B | PiT-B | Vis-S |
|------|-----------------|-------|-------------|-------------|-------------|-------------|-------------|-------------|
| ① | AutoAttack [4] | 99.5 | 34.0 | 30.6 | 13.9 | 3.0 | 8.2 | 11.3 |
| | I-FGSM [13] | 99.7 | 36.3 | 34.1 | 18.5 | 6.8 | 11.8 | 14.6 |
| ② | MI [7] | 100.0 | 59.4 | 53.1 | 36.3 | 12.5 | 23.1 | 26.6 |
| | MDCS-MI | 100.0 | 67.2 | 60.3 | 41.3 | 13.4 | 23.3 | 30.8 |
| | VMI [39] | 99.8 | 69.2 | 66.3 | 56.8 | 31.0 | 46.9 | 54.5 |
| | GRA [50] | 97.3 | 85.2 | 84.3 | 81.3 | 44.6 | 62.2 | 72.9 |
| | MUMODIG [32] | 98.9 | 86.4 | 84.5 | 80.2 | 46.3 | 65.5 | 75.6 |
| | PGN [12] | 98.9 | 88.4 | 86.9 | 85.4 | 49.1 | 68.2 | 76.6 |
| | MEF [30] | 99.3 | 94.9 | 94.4 | 91.2 | 65.3 | 81.1 | 88.2 |
| | MDCS-MEF | 100.0 | 96.4 | 95.5 | 93.4 | 58.7 | 78.8 | 91.0 |
| ③ | TI [8] | 97.8 | 57.9 | 46.9 | 38.9 | 15.3 | 16.5 | 23.2 |
| | DI [42] | 98.7 | 71.0 | 66.2 | 57.1 | 27.5 | 39.7 | 49.5 |
| | SIA [40] | 99.5 | 94.5 | 92.6 | 84.3 | 53.6 | 77.2 | 86.5 |
| | BSR [37] | 99.1 | 97.2 | 96.2 | 89.7 | 56.0 | 80.8 | 89.2 |
| | OPS [14] | 99.5 | 98.0 | 97.8 | 98.2 | 88.8 | 93.8 | 96.7 |
| | MDCS-OPS | 99.9 | 98.9 | 99.0 | 99.1 | 89.3 | 94.7 | 97.9 |

Table 2. The success rates (%) of adversarial attacks against ensemble models.

| Attack | Inc-v3 | Res34 | Inc-v4 | IncRes-v2 |
|-----------------|--------|-------|-------------|-------------|
| SVRE [43] | 99.5 | 100.0 | 74.6 | 65.9 |
| AdaEA [1] | 99.6 | 100.0 | 72.4 | 64.7 |
| MI | 99.6 | 100.0 | 75.6 | 67.0 |
| MDCS-MI | 99.9 | 100.0 | 79.3 | 73.5 |
| MEF | 99.9 | 100.0 | 97.1 | 95.2 |
| MDCS-MEF | 100.0 | 100.0 | 97.9 | 96.6 |
| OPS | 99.9 | 100.0 | 99.7 | 99.6 |
| MDCS-OPS | 100.0 | 100.0 | 99.9 | 99.8 |

counterparts. As expected, the performance for all methods demonstrates a strong positive correlation with the magnitude of ϵ . More critically, the integration of our MDCS module yields a consistent and significant performance enhancement across the entire range of ϵ values for both backbones. MDCS-MI consistently outperforms MI-FGSM, and similarly, MDCS-OPS maintains a clear advantage over OPS. The inset at $\epsilon = 16/255$ highlights this superiority even near saturation. These results affirm that the effectiveness of our MDCS module is not confined to a specific perturbation budget but offers robust improvements, underscoring its general applicability and effectiveness in boosting adversarial attacks.

Fig. 4 presents a comparative analysis of two baseline attacks, MI-FGSM and OPS, against their MDCS-enhanced

Table 3. The success rates (%) of adversarial attacks against defended models and adversarially trained models.

| Attack | Inc-v3 _{ens3} | Inc-v3 _{ens4} | IncRes-v2 _{ens} | AT | JPEG | HGD | RS | Bit-Red |
|-----------------|------------------------|------------------------|--------------------------|-------------|-------------|-------------|-------------|-------------|
| MI | 22.0 | 22.5 | 14.9 | 40.7 | 50.2 | 17.4 | 27.5 | 38.9 |
| MDCS-MI | 23.7 | 24.2 | 16.3 | 41.1 | 52.2 | 16.2 | 27.8 | 42.6 |
| MEF | 73.6 | 71.6 | 66.3 | 45.4 | 86.2 | 74.5 | 37.4 | 81.2 |
| MDCS-MEF | 74.5 | 71.5 | 66.3 | 45.5 | 88.5 | 74.6 | 37.2 | 84.7 |
| OPS | 96.8 | 96.7 | 95.3 | 58.3 | 98.5 | 97.2 | 65.3 | 98.1 |
| MDCS-OPS | 97.5 | 97.5 | 96.0 | 58.5 | 98.9 | 98.0 | 66.6 | 99.0 |

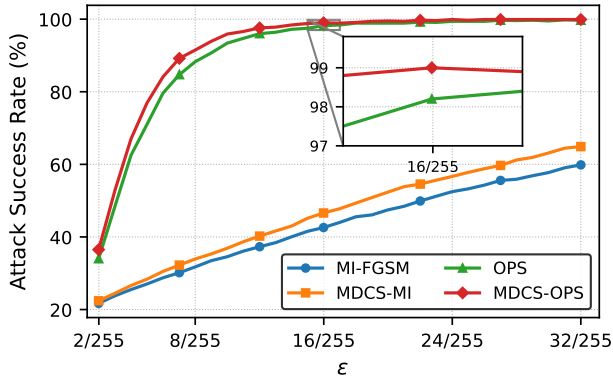


Figure 4. Ablation study on the value of ϵ . We employ Res50 as surrogate model and Inc-v3 as target model.

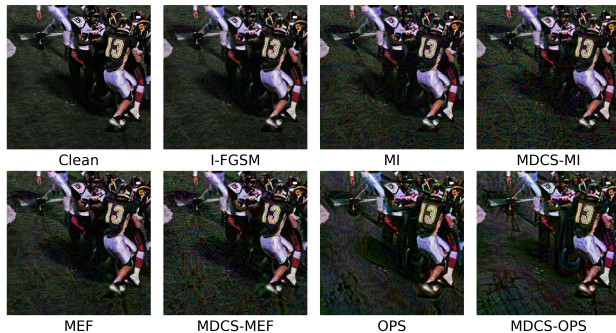


Figure 5. Visualization of AEs on image classification tasks. AEs are crafted on ViT-B/16 with $\epsilon = 16/255$.

4.2. Evaluation on Cross-Modal Retrieval Tasks

Image-Text cross-modal retrieval addresses the task of retrieving the most relevant top-ranked results from a gallery of one modality, given a query from a different modality [2, 41]. To demonstrate the broader applicability of our MDCS strategy, we further investigate its potential to enhance state-of-the-art multimodal attacks on retrieval tasks.

Following [11, 26], we focus on assessing the transferability of AEs across widely adopted VLM architectures: fused and aligned, including ALBEF, TCL, CLIP_{CNN}, CLIP_{ViT}. We leverage Flickr30K and MSCOCO datasets

[24, 45] for evaluating the cross-modal retrieval task. We adopt PGD, Sep-Attack (separate unimodal attack), Co-Attack [46], SGA [26], DRA [11], SA-AET [17] as our baselines. It can be noticed that these baseline frameworks still rely on conventional sign-based optimizers (e.g., PGD) for the underlying perturbation generation. We hypothesize that replacing the standard optimizer with our theoretically grounded MDCS can improve the stability of the optimization process within these frameworks, thereby unlocking greater black-box transferability. To validate this, we integrate our MDCS strategy into the SGA, DRA, and SA-AET frameworks separately, creating enhanced variants: MDCS-SGA, MDCS-DRA, and MDCS-SAAET.

As shown in Tab. 4, integrating our MDCS consistently and significantly boosts the success rates of state-of-the-art attacks (SGA, DRA, SA-AET) across all evaluated models. We summarize three key findings: (1) MDCS is particularly effective against CLIP-based models. For instance, in the challenging cross-architecture transfer from CLIP_{CNN} to TCL, it elevates the IR R@1 of SA-AET by 8.22% (from 25.18% to 33.40%). (2) The performance gains on TR are often more pronounced than on IR. When transferring from CLIP_{ViT} to ALBEF, MDCS brings a +6.37% improvement in TR versus +4.58% in IR. (3) The benefits of MDCS are complementary to state-of-the-art attacks. While SA-AET is already a strong baseline, MDCS-SAAET further pushes the TR R@1 from 54.23% to 60.25% against CLIP_{ViT}. These results collectively affirm MDCS as a highly effective, model-agnostic, and plug-and-play module for boosting adversarial transferability.

We also provide a visualization of our generated AEs on retrieval tasks in Fig. 6. As shown, the generated adversarial perturbations by MDCS-SAAET are imperceptible.

5. Conclusion

This paper addresses the issues of non-convergence and instability in sign-based adversarial attacks. From an optimization perspective, we develop a series of novel optimizers that incorporate the MDCS strategy to improve both stability and transferability. Specifically, we prove that MI-FGSM equipped with MDCS achieves the optimal convergence rate. Experimental results on image classification and

Table 4. The adversarial attacks against multimodal models on Flickr30K dataset. The source model column shows VLMs we use to generate multimodal AEs. The gray area represents adversarial attacks under a white-box setting; the rest are black-box attacks. R@1 denotes the attack success rate at the top-1 rank. The adversarial perturbation is set to 8/255, with a per-step size of 2/255, and a total of 10 iterations. For both Image-Text Retrieval (TR) and Text-Image Retrieval (IR), we provide R@1 scores here. More results are listed in the Supplementary Material (Sec. 8.3).

| Source | Attack | ALBEF | | TCL | | CLIP _{VIT} | | CLIP _{CNN} | |
|---------------------|-------------------|--------------|--------------|--------------|--------------|---------------------|--------------|---------------------|--------------|
| | | TR R@1 | IR R@1 | TR R@1 | IR R@1 | TR R@1 | IR R@1 | TR R@1 | IR R@1 |
| ALBEF | PGD | 52.45 | 58.65 | 3.06 | 6.79 | 8.96 | 13.21 | 10.34 | 14.65 |
| | Sep-Attack | 65.69 | 73.95 | 17.60 | 32.95 | 31.17 | 45.21 | 32.82 | 45.49 |
| | Co-Attack | 97.08 | 98.36 | 39.52 | 51.24 | 29.82 | 38.92 | 31.29 | 41.99 |
| | SGA | 99.79 | 99.95 | 87.67 | 87.88 | 38.04 | 46.17 | 41.63 | 50.36 |
| | MDCS-SGA | 100.0 | 99.98 | 91.78 | 91.24 | 41.35 | 49.71 | 45.08 | 53.93 |
| | DRA | 99.79 | 99.91 | 89.78 | 90.52 | 46.63 | 57.28 | 50.32 | 59.11 |
| | MDCS-DRA | 99.90 | 99.98 | 93.26 | 92.98 | 49.94 | 59.31 | 55.56 | 62.44 |
| | SA-AET | 99.90 | 100.0 | 96.31 | 96.19 | 54.23 | 63.50 | 58.88 | 65.18 |
| | MDCS-SAAET | 99.90 | 100.0 | 96.52 | 96.71 | 60.25 | 67.01 | 60.54 | 67.89 |
| TCL | PGD | 6.15 | 10.78 | 77.87 | 79.84 | 10.18 | 16.31 | 14.81 | 21.11 |
| | Sep-Attack | 20.13 | 36.48 | 84.72 | 86.10 | 31.29 | 44.65 | 33.33 | 45.80 |
| | Co-Attack | 49.84 | 60.36 | 91.68 | 95.48 | 32.64 | 42.69 | 32.06 | 47.82 |
| | SGA | 93.33 | 92.84 | 100.0 | 100.0 | 37.42 | 46.39 | 42.02 | 51.36 |
| | MDCS-SGA | 95.10 | 94.69 | 100.0 | 100.0 | 42.45 | 49.19 | 46.87 | 55.71 |
| | DRA | 95.31 | 95.35 | 100.0 | 100.0 | 46.26 | 56.80 | 50.70 | 61.54 |
| | MDCS-DRA | 96.66 | 96.42 | 100.0 | 100.0 | 50.92 | 59.76 | 56.19 | 65.01 |
| | SA-AET | 98.85 | 98.48 | 100.0 | 99.98 | 53.99 | 63.27 | 59.64 | 68.44 |
| | MDCS-SAAET | 99.17 | 98.88 | 100.0 | 100.0 | 57.79 | 65.98 | 62.71 | 71.01 |
| CLIP _{VIT} | PGD | 3.13 | 6.48 | 4.85 | 8.17 | 69.33 | 84.79 | 13.03 | 17.43 |
| | Sep-Attack | 7.61 | 20.58 | 10.12 | 20.20 | 76.92 | 87.44 | 29.89 | 38.32 |
| | Co-Attack | 8.55 | 20.18 | 10.01 | 21.29 | 78.5 | 87.50 | 29.50 | 38.49 |
| | SGA | 21.58 | 34.89 | 24.66 | 35.83 | 100.0 | 100.0 | 52.49 | 60.38 |
| | MDCS-SGA | 29.30 | 40.69 | 30.56 | 39.81 | 100.0 | 100.0 | 57.60 | 66.00 |
| | DRA | 27.95 | 43.29 | 29.08 | 44.83 | 100.0 | 100.0 | 62.45 | 69.47 |
| | MDCS-DRA | 34.41 | 48.15 | 35.51 | 48.40 | 100.0 | 100.0 | 68.45 | 73.41 |
| | SA-AET | 35.97 | 50.28 | 37.93 | 51.36 | 100.0 | 100.0 | 69.09 | 74.00 |
| | MDCS-SAAET | 42.34 | 54.86 | 43.52 | 55.45 | 100.0 | 100.0 | 73.18 | 77.53 |
| CLIP _{CNN} | PGD | 2.29 | 6.15 | 4.53 | 8.88 | 5.41 | 12.08 | 89.78 | 92.25 |
| | Sep-Attack | 9.38 | 22.99 | 11.28 | 25.45 | 26.13 | 39.24 | 93.61 | 95.31 |
| | Co-Attack | 10.53 | 23.62 | 12.54 | 26.05 | 27.24 | 40.62 | 95.91 | 96.50 |
| | SGA | 15.02 | 28.60 | 18.34 | 32.26 | 39.51 | 51.16 | 100.0 | 100.0 |
| | MDCS-SGA | 19.19 | 33.44 | 23.92 | 36.48 | 45.89 | 56.22 | 99.87 | 100.0 |
| | DRA | 19.08 | 33.96 | 22.02 | 37.45 | 48.34 | 59.02 | 100.0 | 99.93 |
| | MDCS-DRA | 23.04 | 39.43 | 25.82 | 41.05 | 55.83 | 63.89 | 100.0 | 100.0 |
| | SA-AET | 23.88 | 37.89 | 25.18 | 41.69 | 54.60 | 63.14 | 100.0 | 99.97 |
| | MDCS-SAAET | 30.76 | 45.02 | 33.40 | 47.57 | 61.72 | 69.56 | 100.0 | 99.97 |

cross-modal retrieval tasks demonstrate that MDCS serves as a universal strategy, seamlessly integrating with existing sign-based attacks and significantly enhancing their transferability and stability.

References

- [1] Bin Chen, Shukai Chen Jia-Li Yin, Bo-Hao Chen, and Ximeng Liu. An adaptive model ensemble adversarial attack for boosting adversarial transferability. In *ICCV*, 2023. 5, 6
- [2] Hui Chen, Guiguang Ding, Xudong Liu, Zijia Lin, Ji Liu, and Jungong Han. Imram: Iterative matching with recurrent attention memory for cross-modal image-text retrieval. In *Proceedings of the IEEE/CVF conference on computer vision and pattern recognition*, pages 12655–12663, 2020. 7
- [3] Zhensu Chen, Lingxi Xie, Jianwei Niu, Xuefeng Liu, Longhui Wei, and Qi Tian. Visformer: The vision-friendly transformer. In *Proceedings of the IEEE/CVF international*



Figure 6. Visualization of AEs on image-text retrieval tasks with MDCS-SAAET. AEs are crafted on ALBEF and are constrained by an L_∞ norm of $8/255$, generated over 10 iterations with a step size of $2/255$.

- conference on computer vision, pages 589–598, 2021. 5
- [4] Francesco Croce and Matthias Hein. Reliable evaluation of adversarial robustness with an ensemble of diverse parameter-free attacks. In *ICML*, 2020. 6
- [5] Xuanming Cui, Alejandro Aparcedo, Young Kyun Jang, and Ser-Nam Lim. On the robustness of large multimodal models against image adversarial attacks. In *Proceedings of the IEEE/CVF Conference on Computer Vision and Pattern Recognition*, pages 24625–24634, 2024. 1, 3
- [6] Bertsekas Dimitri P., Nedic Angelia., and Ozdaglar Asuman E. *Convex analysis and optimization*. Athena Scientific, 2003. 2
- [7] Yinpeng Dong, Fangzhou Liao, Tianyu Pang, Hang Su, Jun Zhu, Xiaolin Hu, and Jianguo Li. Boosting adversarial attacks with momentum. In *CVPR*, 2018. 1, 3, 5, 6
- [8] Yinpeng Dong, Tianyu Pang, Hang Su, and Jun Zhu. Evading defenses to transferable adversarial examples by translation-invariant attacks. In *CVPR*, 2019. 3, 6
- [9] Alexey Dosovitskiy, Lucas Beyer, Alexander Kolesnikov, Dirk Weissenborn, and Xiaohua Zhai. An image is worth 16x16 words: Transformers for image recognition at scale. In *ICLR*, 2021. 5
- [10] John C. Duchi, Elad Hazan, and Yoram Singer. Adaptive subgradient methods for online learning and stochastic optimization. In *J. Mach. Learn. Res.*, 2010. 2
- [11] Sensen Gao, Xiaojun Jia, Xuhong Ren, Ivor Tsang, and Qing Guo. Boosting transferability in vision-language attacks via diversification along the intersection region of adversarial trajectory. In *European Conference on Computer Vision*, pages 442–460. Springer, 2024. 1, 3, 7
- [12] Zhijin Ge, Xiaosen Wang, Hongying Liu, Fanhua Shang, and Yuanyuan Liu. Boosting adversarial transferability by achieving flat local maxima. In *NeurIPS*, 2023. 1, 3, 5, 6
- [13] Ian J. Goodfellow, Jonathon Shlens, and Christian Szegedy. Explaining and harnessing adversarial examples. In *ICLR*, 2015. 1, 3, 6
- [14] Yu Guo, Weiquan Liu, Qingshan Xu, Shijun Zheng, Shujun Huang, Yu Zang, Siqi Shen, Chenglu Wen, and Cheng Wang. Boosting adversarial transferability through augmentation in hypothesis space. In *Proceedings of the Computer Vision and Pattern Recognition Conference*, pages 19175–19185, 2025. 3, 5, 6
- [15] Byeongho Heo, Sangdoon Yun, Dongyoon Han, Sanghyuk Chun, Junsuk Choe, and Seong Joon Oh. Rethinking spatial dimensions of vision transformers. In *Proceedings of the IEEE/CVF international conference on computer vision*, pages 11936–11945, 2021. 5
- [16] Martin Heusel, Hubert Ramsauer, Thomas Unterthiner, Bernhard Nessler, and Sepp Hochreiter. Gans trained by a two time-scale update rule converge to a local nash equilibrium. In *Neurips*, 2017. 3
- [17] Xiaojun Jia, Sensen Gao, Qing Guo, Simeng Qin, Ke Ma, Yihao Huang, Yang Liu, Ivor Tsang, and Xiaochun Cao. Semantic-aligned adversarial evolution triangle for high-transferability vision-language attack. *IEEE Transactions on Pattern Analysis and Machine Intelligence*, 2025. 1, 3, 7
- [18] Siddharth Karamcheti, Suraj Nair, Ashwin Balakrishna, Percy Liang, Thomas Kollar, and Dorsa Sadigh. Prismatic vlms: Investigating the design space of visually-conditioned language models. In *ICLR*, 2024. 3
- [19] Sai Praneeth Karimireddy, Quentin Rebjock, Sebastian U. Stich, and Martin Jaggi. Error feedback fixes signsgd and other gradient compression schemes. In *ICML*, 2019. 1
- [20] Diederik P. Kingma and Jimmy Ba. Adam: A method for stochastic optimization. In *ICLR*, 2015. 2, 4
- [21] Alexey Kurakin, Ian J. Goodfellow, and Samy Bengio. Adversarial examples in the physical world. In *ICLR Workshop*, 2017. 1, 3
- [22] Qizhang Li, Yiwen Guo, Wangmeng Zuo, and Hao Chen. Improving adversarial transferability via intermediate-level perturbation decay. In *NeurIPS*, 2023. 5
- [23] Jiadong Lin, Chuanbiao Song, Kun He, Liwei Wang, and John E. Hopcroft. Nesterov accelerated gradient and scale invariance for adversarial attacks. In *ICLR*, 2020. 3, 5
- [24] Tsung-Yi Lin, Michael Maire, Serge Belongie, James Hays, Pietro Perona, Deva Ramanan, Piotr Dollár, and C Lawrence Zitnick. Microsoft coco: Common objects in context. In *European conference on computer vision*, pages 740–755. Springer, 2014. 7
- [25] Haotian Liu, Chunyuan Li, Yuheng Li, and Yong Jae Lee. Improved baselines with visual instruction tuning. In *CVPR*, pages 26296–26306, 2024. 3
- [26] Dong Lu, Zhiqiang Wang, Teng Wang, Weili Guan, Hongchang Gao, and Feng Zheng. Set-level guidance attack: Boosting adversarial transferability of vision-language pre-training models. In *Proceedings of the IEEE/CVF International Conference on Computer Vision*, pages 102–111, 2023. 1, 3, 7
- [27] Aleksander Madry, Aleksandar Makelov, Ludwig Schmidt, Dimitris Tsipras, and Adrian Vladu. Towards deep learning models resistant to adversarial attacks. In *ICLR*, 2018. 1, 3
- [28] Mahesh Chandra Mukkamala and Matthias Hein. Variants of rmsprop and adagrad with logarithmic regret bounds. In *ICLR*, 2017. 1
- [29] Boris Polyak. Some methods of speeding up the convergence of iteration methods. *Ussr Computational Mathematics and Mathematical Physics*, 4:1–17, 1964. 1, 3

- [30] Chunlin Qiu, Yiheng Duan, Lingchen Zhao, and Qian Wang. Enhancing adversarial transferability through neighborhood conditional sampling. *ArXiv*, abs/2405.16181, 2024. 1, 3, 5, 6
- [31] Sashank J Reddi, Satyen Kale, and Sanjiv Kumar. On the convergence of adam and beyond. In *ICLR*, 2018. 2, 4, 5
- [32] Yuchen Ren, Zhengyu Zhao, Chenhao Lin, Bo Yang, Lu Zhou, Zhe Liu, and Chao Shen. Improving integrated gradient-based transferable adversarial examples by refining the integration path. In *Proceedings of the AAAI Conference on Artificial Intelligence*, pages 6731–6739, 2025. 1, 6
- [33] Amanpreet Singh, Vivek Natarjan, Meet Shah, Yu Jiang, Xinlei Chen, Dhruv Batra, Devi Parikh, and Marcus Rohrbach. Towards vqa models that can read. In *Proceedings of the IEEE Conference on Computer Vision and Pattern Recognition*, pages 8317–8326, 2019. 3
- [34] Chawin Sitawarin. New perspectives on adversarially robust machine learning systems. *Technical Report No. UCB/EECS-2024-10*, 2024. 3
- [35] Wei Tao, Sheng Long, Gaowei Wu, and Qing Tao. The role of momentum parameters in the optimal convergence of adaptive polyak’s heavy-ball methods. In *ICLR*, 2021. 5
- [36] Guanghui Wang, Shiyin Lu, Weiwei Tu, and Lijun Zhang. Sadam: A variant of adam for strongly convex functions. In *ICLR*, 2020. 5
- [37] Kunyu Wang, Xuanran He, Wenxuan Wang, and Xiaosen Wang. Boosting adversarial transferability by block shuffle and rotation. In *Proceedings of the IEEE/CVF conference on computer vision and pattern recognition*, pages 24336–24346, 2024. 3, 6
- [38] Xiaosen Wang, Xuanran He, Jingdong Wang, and Kun He. Admix: Enhancing the transferability of adversarial attacks. In *ICCV*, 2021. 3
- [39] Xiaosen Wang, Jiadong Lin, Han Hu, Jingdong Wang, and Kun He. Boosting adversarial transferability through enhanced momentum. In *BMVC*, 2021. 1, 3, 5, 6
- [40] Xiaosen Wang, Zeliang Zhang, and Jianping Zhang. Structure invariant transformation for better adversarial transferability. In *Proceedings of the IEEE/CVF International Conference on Computer Vision*, pages 4607–4619, 2023. 6
- [41] Zihao Wang, Xihui Liu, Hongsheng Li, Lu Sheng, Junjie Yan, Xiaogang Wang, and Jing Shao. Camp: Cross-modal adaptive message passing for text-image retrieval. In *Proceedings of the IEEE/CVF international conference on computer vision*, pages 5764–5773, 2019. 7
- [42] Cihang Xie, Zhishuai Zhang, Jianyu Wang, Yuyin Zhou, Zhou Ren, and Alan Loddon Yuille. Improving transferability of adversarial examples with input diversity. *2019 IEEE/CVF Conference on Computer Vision and Pattern Recognition (CVPR)*, pages 2725–2734, 2019. 3, 6
- [43] Yifeng Xiong, Jiadong Lin, Min Zhang, John E. Hopcroft, and Kun He. Stochastic variance reduced ensemble adversarial attack for boosting the adversarial transferability. In *CVPR*, 2022. 5, 6
- [44] Ziyi Yin, Muchao Ye, Tianrong Zhang, Jiaqi Wang, Han Liu, Jinghui Chen, Ting Wang, and Fenglong Ma. Vqattack: Transferable adversarial attacks on visual question answering via pre-trained models. In *Proceedings of the AAAI Conference on Artificial Intelligence*, pages 6755–6763, 2024. 3
- [45] Peter Young, Alice Lai, Micah Hodosh, and Julia Hockenmaier. From image descriptions to visual denotations: New similarity metrics for semantic inference over event descriptions. *Transactions of the Association for Computational Linguistics*, 2:67–78, 2014. 7
- [46] Jiaming Zhang, Qi Yi, and Jitao Sang. Towards adversarial attack on vision-language pre-training models. In *Proceedings of the 30th ACM International Conference on Multimedia*, pages 5005–5013, 2022. 1, 3, 7
- [47] Richard Zhang, Phillip Isola, Alexei A Efros, Eli Shechtman, and Oliver Wang. The unreasonable effectiveness of deep features as a perceptual metric. In *Proceedings of the IEEE conference on computer vision and pattern recognition*, pages 586–595, 2018. 3
- [48] Zhengyu Zhao, Zhuoran Liu, and Martha Larson. Towards large yet imperceptible adversarial image perturbations with perceptual color distance. In *Proceedings of the IEEE/CVF conference on computer vision and pattern recognition*, pages 1039–1048, 2020. 3
- [49] Zhengyu Zhao, Hanwei Zhang, Renjue Li, Ronan Sicre, Laurent Amsaleg, Michael Backes, Qi Li, Qian Wang, and Chao Shen. Revisiting transferable adversarial images: Systemization, evaluation, and new insights. *IEEE Transactions on Pattern Analysis and Machine Intelligence*, 2025. 3
- [50] Hegui Zhu, Yuchen Ren, Xiaoyan Sui, Lianping Yang, and Wuming Jiang. Boosting adversarial transferability via gradient relevance attack. In *CVPR*, 2023. 1, 2, 3, 6

The Power of Decaying Steps: Enhancing Attack Stability and Transferability for Sign-based Optimizers

Supplementary Material

6. Convergence Analysis of MDCS-MI

Lemma 4. [28] $\forall \mathbf{x}_1, \mathbf{x}_2 \in \mathbb{R}^d$, we have

$$\|P_{\mathbf{Q}, \mathbf{D}_t^{-1}}(\mathbf{x}_1) - P_{\mathbf{Q}, \mathbf{D}_t^{-1}}(\mathbf{x}_2)\|_{\mathbf{D}_t^{-1}} \leq \|\mathbf{x}_1 - \mathbf{x}_2\|_{\mathbf{D}_t^{-1}}. \quad (11)$$

and

$$\mathbf{x}^* = P_{\mathbf{Q}, \mathbf{D}_t^{-1}}(\mathbf{x}^*). \quad (12)$$

Lemma 5. Let $1 > \lambda > 0$ and $\beta > 0$. Let $\beta_t = \beta\lambda^{t-1}$. Suppose $\{\mathbf{m}_{t+1}\}_{t=1}^{\infty}$ is generated by MDCS-MI. Then there exists a $M_2 > 1$ such that

$$\|\mathbf{m}_{t+1}\| \leq M_2, \quad \forall t > 0,$$

Proof Note

$$\|\nabla_{\mathbf{x}} J(\mathbf{x}^{adv})\| \leq \|\nabla_{\mathbf{x}} J(\mathbf{x}^{adv})\|_1.$$

Then

$$\|\mathbf{m}_{t+1}\| \leq \beta_t \|\mathbf{m}_t\| + 1 \leq \beta_{t-1} \|\mathbf{m}_{t-1}\| + \beta_t + 1 \leq \sum_{i=1}^t \beta_i + 1.$$

Let $M_2 = \sum_{i=1}^{\infty} \beta_i + 1$, Lemma 5 follows from the convergence of $\sum_{i=1}^t \beta_i$.

Note

$$d_{t,i} = \min\left(\frac{1}{\|\mathbf{m}_{t+1,i}\|}, d_{t-1,i}\right).$$

According to Lemma 5, we can get

Lemma 6. Let $1 > \lambda > 0$ and $\beta > 0$. Let $\beta_t = \beta\lambda^{t-1}$. Suppose $\{\mathbf{D}_t\}_{t=1}^{\infty}$ is generated by MDCS-MI. Then for each t and i ,

$$\frac{1}{M_2} \leq d_{t,i} \leq 1.$$

Proof of Theorem 3

From Lemma 4, we know

$$\begin{aligned} & \|\mathbf{x}_{t+1}^{adv} - \mathbf{x}^*\|_{\mathbf{D}_t^{-1}}^2 \\ &= \|P_{\mathbf{Q}, \mathbf{D}_t^{-1}}(\mathbf{x}_t^{adv} + \alpha_t \mathbf{D}_t \mathbf{m}_{t+1}) - P_{\mathbf{Q}, \mathbf{D}_t^{-1}}(\mathbf{x}^*)\|_{\mathbf{D}_t^{-1}}^2 \\ &\leq \|\mathbf{x}_t^{adv} + \alpha_t \mathbf{D}_t \mathbf{m}_{t+1} - \mathbf{x}^*\|_{\mathbf{D}_t^{-1}}^2 \\ &= \|\mathbf{x}_t^{adv} - \mathbf{x}^*\|_{\mathbf{D}_t^{-1}}^2 + \|\alpha_t \mathbf{D}_t \mathbf{m}_{t+1}\|_{\mathbf{D}_t^{-1}}^2 \\ &\quad + 2\alpha_t \langle \mathbf{m}_{t+1}, \mathbf{x}_t^{adv} - \mathbf{x}^* \rangle \\ &= \|\mathbf{x}_t^{adv} - \mathbf{x}^*\|_{\mathbf{D}_t^{-1}}^2 + \|\alpha_t \mathbf{D}_t \mathbf{m}_{t+1}\|_{\mathbf{D}_t^{-1}}^2 \\ &\quad + 2\alpha_t \langle \beta_t \mathbf{m}_t + \frac{\nabla_{\mathbf{x}} J(\mathbf{x}_t^{adv})}{\|\nabla_{\mathbf{x}} J(\mathbf{x}_t^{adv})\|_1}, \mathbf{x}_t^{adv} - \mathbf{x}^* \rangle. \end{aligned}$$

Rearrange the inequality, we have

$$\begin{aligned} & \frac{2\alpha_t}{\|\nabla_{\mathbf{x}} J(\mathbf{x}_t^{adv})\|_1} \langle \nabla_{\mathbf{x}} J(\mathbf{x}_t^{adv}), \mathbf{x}_t^{adv} - \mathbf{x}^* \rangle \\ & \geq \|\mathbf{x}_{t+1}^{adv} - \mathbf{x}^*\|_{\mathbf{D}_t^{-1}}^2 - \|\mathbf{x}_t^{adv} - \mathbf{x}^*\|_{\mathbf{D}_t^{-1}}^2 \\ & \quad - \|\alpha_t \mathbf{D}_t \mathbf{m}_{t+1}\|_{\mathbf{D}_t^{-1}}^2 - 2\alpha_t \beta_t \langle \mathbf{m}_t, \mathbf{x}_t^{adv} - \mathbf{x}^* \rangle, \end{aligned}$$

i.e.,

$$\begin{aligned} & \frac{1}{\|\nabla_{\mathbf{x}} J(\mathbf{x}_t^{adv})\|_1} \langle \nabla_{\mathbf{x}} J(\mathbf{x}_t^{adv}), \mathbf{x}_t^{adv} - \mathbf{x}^* \rangle \\ & \geq \frac{\|\mathbf{x}_{t+1}^{adv} - \mathbf{x}^*\|_{\mathbf{D}_t^{-1}}^2 - \|\mathbf{x}_t^{adv} - \mathbf{x}^*\|_{\mathbf{D}_t^{-1}}^2}{2\alpha_t} - \frac{\alpha_t \|\mathbf{m}_{t+1}\|^2}{2} \\ & \quad - \beta_t \langle \mathbf{m}_t, \mathbf{x}_t^{adv} - \mathbf{x}^* \rangle \\ & \geq \frac{\|\mathbf{x}_{t+1}^{adv} - \mathbf{x}^*\|_{\mathbf{D}_t^{-1}}^2 - \|\mathbf{x}_t^{adv} - \mathbf{x}^*\|_{\mathbf{D}_t^{-1}}^2}{2\alpha_t} - \frac{\alpha_t \|\mathbf{m}_{t+1}\|^2}{2} \\ & \quad - \frac{\beta_t \alpha_t \|\mathbf{m}_t\|^2}{2} - \frac{\beta_t \|\mathbf{x}_t^{adv} - \mathbf{x}^*\|^2}{2\alpha_t}. \end{aligned}$$

Using the property of concave functions,

$$\langle \nabla_{\mathbf{x}} J(\mathbf{x}_t^{adv}), \mathbf{x}_t^{adv} - \mathbf{x}^* \rangle \leq J(\mathbf{x}_t^{adv}) - J(\mathbf{x}^*).$$

Then

$$\begin{aligned} & \frac{J(\mathbf{x}^*) - J(\mathbf{x}_t^{adv})}{M} \\ & \leq \frac{\|\mathbf{x}_t^{adv} - \mathbf{x}^*\|_{\mathbf{D}_t^{-1}}^2 - \|\mathbf{x}_{t+1}^{adv} - \mathbf{x}^*\|_{\mathbf{D}_t^{-1}}^2}{2\alpha_t} \\ & \quad + \frac{\alpha_t \|\mathbf{m}_{t+1}\|^2}{2} + \frac{\beta_t \alpha_t \|\mathbf{m}_t\|^2}{2} + \frac{\beta_t \|\mathbf{x}_t^{adv} - \mathbf{x}^*\|^2}{2\alpha_t}. \end{aligned}$$

Summing this inequality from $t = 1$ to T , we obtain

$$\begin{aligned} & \frac{1}{M} \sum_{t=1}^T [J(\mathbf{x}^*) - J(\mathbf{x}_t^{adv})] \\ & \leq \underbrace{\sum_{t=1}^T \frac{\|\mathbf{x}_t^{adv} - \mathbf{x}^*\|_{\mathbf{D}_t^{-1}}^2 - \|\mathbf{x}_{t+1}^{adv} - \mathbf{x}^*\|_{\mathbf{D}_t^{-1}}^2}{2\alpha_t}}_{P_1} \\ & \quad + \underbrace{\sum_{t=1}^T \frac{\beta_t \|\mathbf{x}_t^{adv} - \mathbf{x}^*\|^2}{2\alpha_t}}_{P_2} \\ & \quad + \underbrace{\sum_{t=1}^T \frac{\alpha_t \|\mathbf{m}_{t+1}\|^2}{2} + \sum_{t=1}^T \frac{\beta_t \alpha_t \|\mathbf{m}_t\|^2}{2}}_{P_3}. \end{aligned}$$

To bound P_1 , we have

$$\begin{aligned}
P_1 &= \sum_{t=1}^T \frac{\|\mathbf{x}_t^{adv} - \mathbf{x}^*\|_{\mathbf{D}_t^{-1}}^2 - \|\mathbf{x}_{t+1}^{adv} - \mathbf{x}^*\|_{\mathbf{D}_t^{-1}}^2}{2\alpha_t} \\
&= \sum_{t=2}^T \left(\frac{\|\mathbf{x}_t^{adv} - \mathbf{x}^*\|_{\mathbf{D}_t^{-1}}^2}{2\alpha_t} - \frac{\|\mathbf{x}_t^{adv} - \mathbf{x}^*\|_{\mathbf{D}_{t-1}^{-1}}^2}{2\alpha_{t-1}} \right) \\
&\quad + \frac{\|\mathbf{x}_1^{adv} - \mathbf{x}^*\|_{\mathbf{D}_1^{-1}}^2}{2\alpha_1} - \frac{\|\mathbf{x}_{T+1}^{adv} - \mathbf{x}^*\|_{\mathbf{D}_T^{-1}}^2}{2\alpha_T}
\end{aligned} \tag{13}$$

According to Lemma 6,

$$\begin{aligned}
P_1 &\leq \sum_{t=2}^T \sum_{i=1}^d \left(\frac{1}{2\alpha_t d_{t,i}} - \frac{1}{2\alpha_{t-1} d_{t-1,i}} \right) \|\mathbf{x}_{t,i}^{adv} - \mathbf{x}_i^*\|^2 \\
&\quad + \frac{\|\mathbf{x}_1^{adv} - \mathbf{x}^*\|_{\mathbf{D}_1^{-1}}^2}{2\alpha_1} \\
&\leq \sum_{i=1}^d \frac{1}{2\alpha_T d_{T,i}} G^2 \\
&\leq \frac{dM_2 G^2 \sqrt{T}}{2\gamma}.
\end{aligned} \tag{14}$$

To bound P_2 , we have

$$\begin{aligned}
P_2 &= \sum_{t=1}^T \frac{\beta_t \|\mathbf{x}_t^{adv} - \mathbf{x}^*\|^2}{2\alpha_t} \\
&\leq \frac{\beta G^2}{2\gamma} \sum_{t=1}^T \lambda^{t-1} \sqrt{t} \\
&\leq \frac{\beta G^2}{2\gamma} \sum_{t=1}^T \lambda^{t-1} t \\
&\leq \frac{\beta G^2}{2\gamma(1-\lambda)^2}
\end{aligned} \tag{15}$$

To bound P_3 , according to Lemma 4, we have

$$\begin{aligned}
P_3 &= \sum_{t=1}^T \frac{\alpha_t \|\mathbf{m}_{t+1}\|^2}{2} + \sum_{t=1}^T \frac{\beta_t \alpha_t \|\mathbf{m}_t\|^2}{2} \\
&\leq \sum_{t=1}^T \frac{\alpha_t M_2^2}{2} + \sum_{t=1}^T \frac{\beta_t \alpha_t M_2^2}{2} \\
&\leq \frac{M_2^2}{2} \sum_{t=1}^T \frac{\gamma}{\sqrt{t}} + \frac{D_2^2}{2} \sum_{t=1}^T \frac{\beta_t \gamma}{\sqrt{t}} \\
&\leq 2\gamma M_2^2 \sqrt{T}.
\end{aligned} \tag{16}$$

Combining (14), (15) and (16), we have

$$\begin{aligned}
&\frac{1}{M} \sum_{t=1}^T (J(\mathbf{x}^*) - J(\mathbf{x}_t^{adv})) \\
&\leq \frac{dM_2 G^2 \sqrt{T}}{2\gamma} + \frac{\beta G^2}{2\gamma(1-\lambda)^2} + 2\gamma M_2^2 \sqrt{T}.
\end{aligned}$$

Thus

$$\begin{aligned}
&\frac{1}{MT} \sum_{t=1}^T (J(\mathbf{x}^*) - J(\mathbf{x}_t^{adv})) \\
&\leq \frac{dM_2 G^2}{2\gamma \sqrt{T}} + \frac{\beta G^2}{2\gamma(1-\lambda)^2} + \frac{2\gamma M_2^2}{\sqrt{T}}.
\end{aligned}$$

By concavity of $J(\mathbf{x})$, we obtain

$$\begin{aligned}
&J(\mathbf{x}^*) - J(\bar{\mathbf{x}}_T^{adv}) \\
&\leq M \left(\frac{dM_2 G^2}{2\gamma \sqrt{T}} + \frac{\beta G^2}{2\gamma(1-\lambda)^2} + \frac{2\gamma M_2^2}{\sqrt{T}} \right).
\end{aligned} \tag{17}$$

This completes the proof of Theorem 3.

7. Pseudocode for MDCS-MEF and MDCS-OPS

For clarity, we give the detailed descriptions of MDCS-MEF (Algorithm 2) and MDCS-OPS (Algorithm 3) for image classification tasks.

Algorithm 2 MDCS-MEF

Input: Loss function J , a raw example \mathbf{x} with ground-truth label y , the perturbation size ϵ , momentum parameter $0 < \beta_t \leq 1$, step-size $\alpha_t > 0$, maximum iteration T , the outer/inner decay factor μ_{outer}/μ_{inner} ; the number of randomly sampled examples, N ; neighborhood radius ξ , exploration radius γ .

- 1: Initialize $\mathbf{x}_0^{adv} = \mathbf{x}$, $d_{0,i} = 1$. $\mathbf{g}_0^{outer} = 0$; $\{\mathbf{g}_{0,n}^{inner}\}_{n=1}^N = 0$; $\mathbf{x}_0^{adv} = \mathbf{x}$; $\alpha = \epsilon/T$
- 2: **repeat**
- 3: $\{\mathbf{x}_{t,n}\}_{n=1}^N \in U_\gamma(\mathbf{x}_t^{adv})$
- 4: $\{\mathbf{x}'_{t,n}\}_{n=1}^N = \{\mathbf{x}_{t,n}\}_{n=1}^N + \xi \cdot \text{sign}(\mathbf{g}_{t,n}^{inner})_{n=1}^N$
- 5: $\{g_{t,n}\}_{n=1}^N = \nabla_{\mathbf{x}} J(\{\mathbf{x}'_{t,i}\}_{i=1}^N)$
- 6: $\{g_{t,n}^{inner}\}_{n=1}^N = \frac{\{g_{t,n}\}_{n=1}^N}{\|\{g_{t,n}\}_{n=1}^N\|_1} - \mu_{inner} \{g_{t,n}^{inner}\}_{n=1}^N$
- 7: $\mathbf{g}_t^{outer} = \mu_{outer} \mathbf{g}_t^{outer} + \frac{1}{N} \sum_{i=1}^N \frac{\{g_{t,n}\}_{n=1}^N}{\|\{g_{t,n}\}_{n=1}^N\|_1}$
- 8: $d_{t,i} = \min(\frac{1}{|g_{t,i}^{outer}|}, d_{t-1,i})$,
- 9: $\mathbf{D}_t = \text{diag}(\mathbf{d}_t)$,
- 10: $\mathbf{x}_{t+1}^{adv} = P_{\mathbf{Q}, \mathbf{D}_t^{-1}}(\mathbf{x}_t^{adv} + \alpha_t \cdot \mathbf{D}_t \cdot \mathbf{g}_t^{outer})$.

11: **until** $t = T$
Output: \mathbf{x}_T^{adv} .

Algorithm 3 MDCS-OPS

Input: Loss function J , a raw example \mathbf{x} with ground-truth label y , the perturbation size ϵ , the maximum iteration T and decay factor μ ; Level list K_{list} ; Radius list R_{list} ; Number of operator samples N_p ; Number of perturbation samples N_e .

```
1: Initialize  $\mathbf{x}_0^{adv} = \mathbf{x}$ ,  $d_{0,i} = 1$ ,  $\alpha = \epsilon/T$ ,  $\mathbf{m}_0 = \mathbf{0}$ ,  $\Delta_0 = 0$ .
2: repeat
3:    $\bar{\mathbf{g}} = \nabla_{\mathbf{x}} J(f(\mathbf{x} + \Delta_i), y)$ .
4:   for  $\delta$  in  $S(D, N_e)$  do
5:     for  $op$  in  $S(P, N_p)$  do
6:        $\bar{\mathbf{g}} = \bar{\mathbf{g}} + \nabla_{\mathbf{x}} J[f(op(\mathbf{x} + \Delta_i + \delta)), y]$ 
7:     end for
8:   end for
9:    $\bar{\mathbf{g}} = \frac{\bar{\mathbf{g}}}{N_e \times N_p + 1}$ .
10:   $\mathbf{m}_{t+1} = \mu \cdot \mathbf{m}_t + \frac{\bar{\mathbf{g}}}{\|\bar{\mathbf{g}}\|_1}$ .
11:   $d_{t,i} = \min(\frac{1}{|\mathbf{m}_{t,i}|}, d_{t-1,i})$ ,
12:   $\mathbf{D}_t = \text{diag}(\mathbf{d}_t)$ ,
13:   $\Delta_{i+1} = P_{\mathbf{Q}, \mathbf{D}_t^{-1}}(\Delta_i + \alpha_t \cdot \mathbf{D}_t \cdot \mathbf{m}_{t+1})$ .
14: until  $t = T$ 
Output:  $\mathbf{x}_T^{adv}$ .
```

8. Additional Experiments

This section presents more experimental results to provide a comprehensive empirical evaluation of the proposed methods on image classification, Visual Question Answering (VQA), and cross-modal retrieval tasks.

8.1. Image Classification Tasks

8.1.1. Transferability and Stability

In this subsection, we extend our evaluation to include additional source models, namely VGG16 and ViT-B/16. The success rates of these transfer attacks are quantified in Tab. 5. The results clearly demonstrate that our derived MDCS strategy consistently enhances adversarial transferability compared to the baseline attacks. Notably, the MDCS-OPS variant achieves the highest attack success rate in the black-box setting, establishing a new state-of-the-art. As shown in Fig. 7, integrating the MDCS strategy into TI and SI significantly enhances the iterative stability of adversarial attacks.

8.1.2. Ablation Study

Here, we investigate the impact of the step-size parameter γ on the performance of MDCS-MI, which governs the trade-off between transferability and imperceptibility. According to [49], there remains a notable lack of consensus and attention regarding the proper metrics for evaluating imperceptibility. A popular proxy measure of imperceptibility is the L_p -norm of the perturbation. It offers a good trade-off between simplicity, mathematical tractability, and practical-

ity in applications [34]. Recent research [48, 49] suggests that it is problematic to solely constrain all attacks with the same L_∞ norm bound without more comprehensive comparisons. Thus, we employ 7 different metrics as the indicators of imperceptibility of the crafted AEs, including the Average L_∞ Distortion (ALD_p), Average L_2 Distortion (ALD_p) [23], Peak Signal-to-Noise Ratio (PSNR), Structural Similarity Index Measure (SSIM), Multi Scale Structural Similarity Index Measure (MS-SSIM), Frechet Inception Distance (FID) [16], Learned Perceptual Image Patch Similarity (LPIPS) [47]. As shown in Fig. 8, the attack successful rate of MDCS-MI increases with the growth of γ (varied within the range of 0.25 to 10). The rate plateaus at around 47% when γ is greater than 2. For imperceptibility, the increase of γ leads to a significant improvement in all metrics except for FID and $\text{ALD}_p(p = \infty)$. Therefore, a holistic assessment with diverse metrics is essential for evaluating the imperceptibility of AEs. By balancing the transferability and imperceptibility in our experiment, γ is determined by simple grid search over the range [2, 4].

8.2. VQA Tasks

VQA serves as a practical application of large multimodal models, in which the model is tasked with generating an open-ended answer from a given image and an associated question. In contrast to adversarial attacks on image classification, white-box attacks for VQA have not achieved satisfactory performance [5, 44]. Therefore, this subsection specifically investigates white-box attacks on VQA, utilizing image perturbation techniques.

We conduct experiments on the TextVQA dataset [33], targeting two representative VLMs: LLaVA-1.5 [25] and PrismVLM [18]. To validate the effect of our MDCS, we focus on attacking visual encoders to generate AEs for LLaVA-1.5 and PrismVLM, respectively. The white-box attack success rates are reported for two input types: Pure (raw textual questions) and OCR (augmented prompts that incorporate both raw questions and OCR-extracted text from the images).

Tab. 6 presents the attack success rates of our method compared to several baselines. MDCS-MI consistently achieves the highest rates across all experimental settings. The performance gain is particularly significant on the PrismVLM model, achieving an improvement of 3.0% and 4.1% in the Pure and OCR settings, respectively. Fig. 9 presents a side-by-side comparison of the images and PrismVLM’s answers on the textVQA dataset before and after being subjected to the MDCS-MI attack.

8.3. Cross-Modal Retrieval Tasks

In the main body of the paper, we reported R@1 attack success rates for cross-model transferability experiments for conciseness. In this subsection, we present the complete

Table 5. Transferability comparisons across different network architectures. AEs are crafted for VGG16 and ViT-B/16. The best results are marked in bold. The gray area represents adversarial attacks under a white-box setting, the rest are black-box attacks.

| Model | Attack | Res50 | VGG16 | Mob-v2 | Inc-v3 | ViT-B | PiT-B | Vis-S |
|-----------------|-----------------|--------------|-------------|-------------|-------------|-------------|-------------|-------|
| VGG16 | I-FGSM | 35.8 | 99.9 | 62.9 | 27.1 | 8.0 | 15.5 | 25.1 |
| | MI | 59.1 | 99.8 | 80.2 | 55.9 | 15.6 | 29.6 | 44.4 |
| | MDCS-MI | 59.5 | 99.8 | 81.0 | 59.9 | 17.5 | 30.3 | 45.9 |
| | VMI | 74.1 | 99.8 | 88.6 | 72.9 | 26.1 | 44.2 | 60.9 |
| | EMI | 74.6 | 100.0 | 90.5 | 69.8 | 21.5 | 38.9 | 57.9 |
| | GRA | 71.3 | 100.0 | 89.9 | 79.6 | 27.0 | 42.7 | 58.0 |
| | MUMODIG | 90.6 | 100.0 | 96.4 | 90.2 | 31.3 | 54.9 | 78.3 |
| | PGN | 72.1 | 100.0 | 89.4 | 80.8 | 28.0 | 44.9 | 58.6 |
| | MEF | 83.0 | 99.9 | 93.9 | 82.8 | 31.9 | 51.6 | 70.3 |
| | MDCS-MEF | 85.7 | 99.9 | 93.5 | 83.9 | 34.8 | 55.8 | 73.3 |
| | SIA | 92.9 | 100.0 | 98.1 | 86.9 | 35.5 | 61.9 | 84.8 |
| | OPS | 97.4 | 100.0 | 99.2 | 99.1 | 63.7 | 80.1 | 93.4 |
| MDCS-OPS | 98.1 | 100.0 | 99.6 | 99.3 | 66.7 | 82.3 | 93.9 | |
| ViT-B/16 | I-FGSM | 18.0 | 37.8 | 35.5 | 25.4 | 99.9 | 29.0 | 28.6 |
| | MI | 41.2 | 63.9 | 58.7 | 47.3 | 100.0 | 50.2 | 51.0 |
| | MDCS-MI | 45.7 | 70.8 | 61.3 | 53.0 | 100.0 | 54.0 | 55.1 |
| | VMI | 54.6 | 68.9 | 64.7 | 56.2 | 100.0 | 67.5 | 67.3 |
| | EMI | 59.3 | 75.9 | 71.8 | 64.7 | 100.0 | 72.2 | 74.7 |
| | GRA | 66.8 | 76.1 | 74.3 | 71.4 | 99.6 | 80.3 | 80.4 |
| | MUMODIG | 73.2 | 78.6 | 77.2 | 75.0 | 99.4 | 83.7 | 82.8 |
| | PGN | 69.8 | 79.4 | 77.4 | 75.4 | 99.6 | 84.2 | 85.2 |
| | MEF | 75.0 | 81.1 | 82.8 | 78.1 | 99.3 | 88.2 | 88.1 |
| | MDCS-MEF | 74.8 | 84.1 | 84.6 | 80.1 | 99.8 | 88.0 | 88.0 |
| | SIA | 84.2 | 86.8 | 86.8 | 78.3 | 99.9 | 91.4 | 91.5 |
| | OPS | 91.2 | 93.8 | 93.9 | 94.4 | 99.3 | 95.9 | 96.0 |
| MDCS-OPS | 93.9 | 95.9 | 96.0 | 96.6 | 99.9 | 97.7 | 98.3 | |

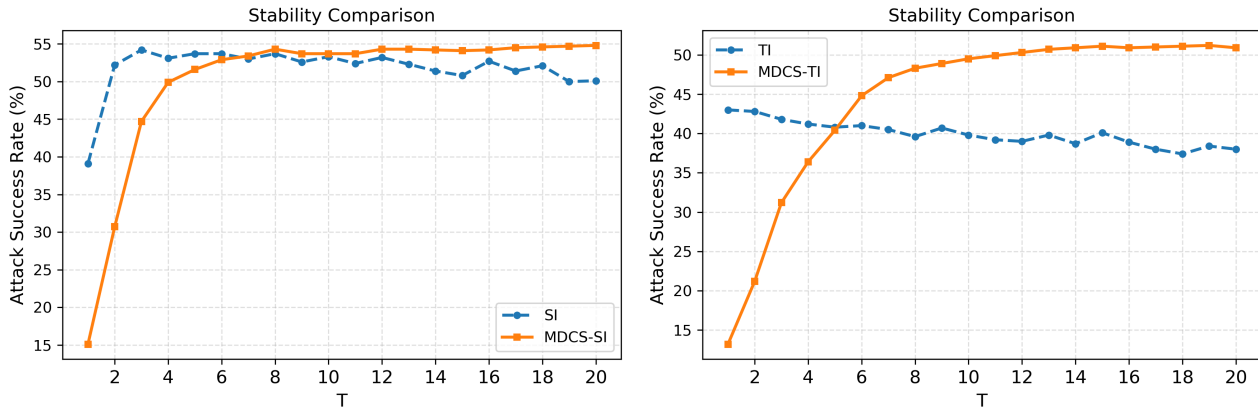


Figure 7. Stability comparison of SI and TI (based on MI-FGSM). We employ Res50 as surrogate model and Inc-v3 as target model with $\epsilon = 16/255$.

evaluation results for both image-text and text-image retrieval tasks on the Flickr30K (Table 7) and MSCOCO (Table 8) datasets. These results include attack success rates at R@1, R@5, and R@10.

These results validate the general applicability of our

MDCS module. Integrating MDCS with a spectrum of attack frameworks, from foundational methods like SGA and DRA to the state-of-the-art SA-AET, yields consistent performance gains. In each tested cross-model transferable scenario, MDCS-SGA, MDCS-DRA, and MDCS-

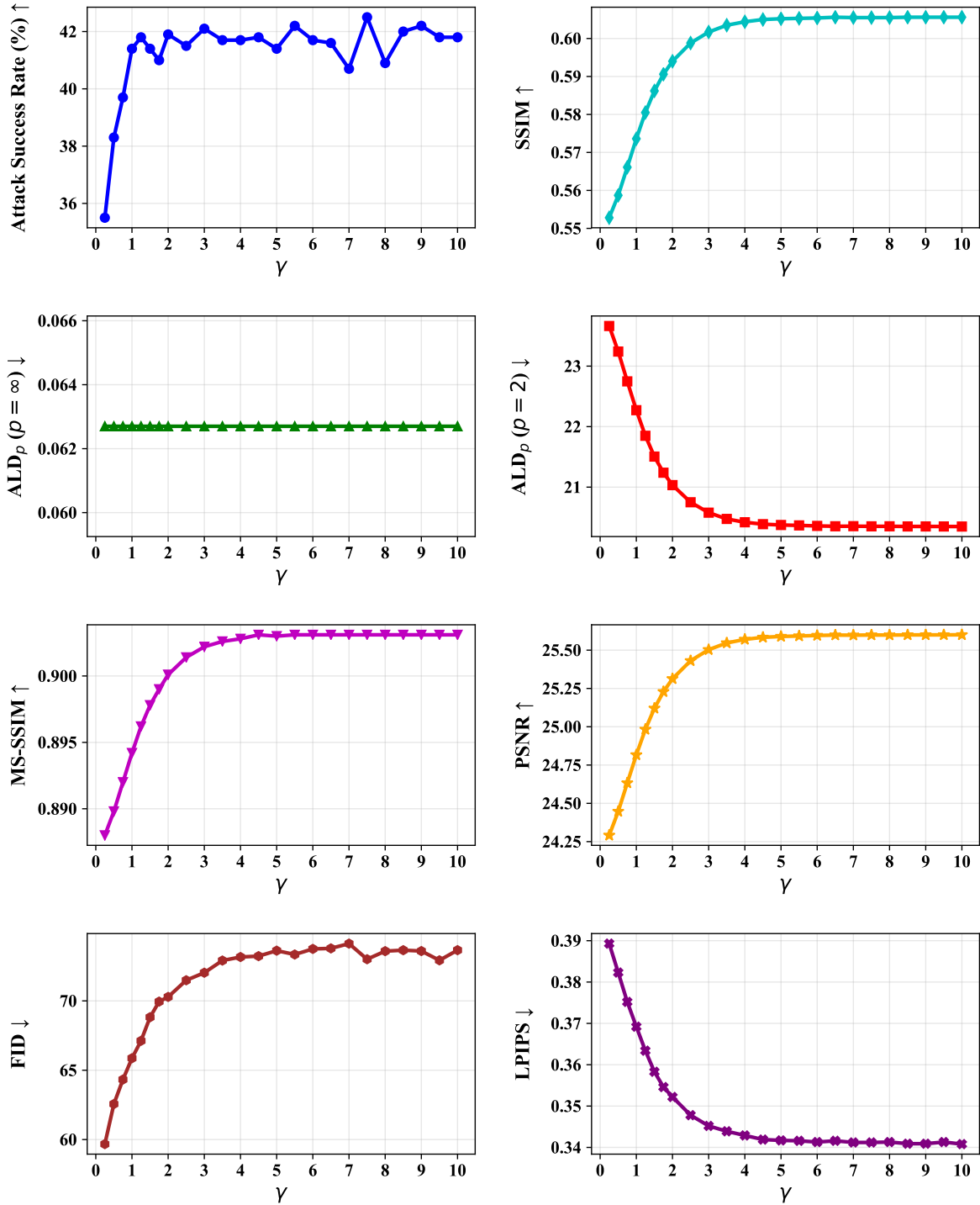


Figure 8. Ablation study on the value of γ for MDCS-MI. We employ Res50 as surrogate model and Inc-v3 as target model.

SAAET demonstrably outperform their baseline counterparts. This confirms that MDCS functions as a potent and model-agnostic component for amplifying the transferability of adversarial attacks across various VLP architectures

and metrics.

Table 6. The white-box adversarial attacks of Pure and OCR VQA tasks in VLMs. The notations Pre, Post_N refer to accuracy (%) for pre-attack, post-attack under normal setting, respectively. ASR represents the Attack Success Rate, which is derived from the values of Pre and Post_N.

| Model | Type | Attack | Pre | Post _N | ASR |
|-----------|------|----------------|------|-------------------|-------------|
| LLaVA-1.5 | Pure | FGSM | 47.3 | 37.2 | 10.1 |
| | | PGD | 47.3 | 22.1 | 25.2 |
| | | MEF | 47.3 | 22.1 | 25.2 |
| | | MI | 47.3 | 20.9 | 26.4 |
| | | MDCS-MI | 47.3 | 20.9 | 26.4 |
| | OCR | FGSM | 58.5 | 53.7 | 4.8 |
| | | PGD | 58.5 | 37.5 | 21.0 |
| | | MEF | 58.5 | 36.3 | 22.2 |
| | | MI | 58.5 | 37.2 | 21.3 |
| | | MDCS-MI | 58.5 | 35.4 | 23.1 |
| PrismVLM | Pure | FGSM | 56.9 | 41.3 | 15.6 |
| | | PGD | 56.9 | 26.1 | 30.8 |
| | | MEF | 56.9 | 25.8 | 31.1 |
| | | MI | 56.9 | 26.0 | 30.9 |
| | | MDCS-MI | 56.9 | 22.8 | 34.1 |
| | OCR | FGSM | 61.9 | 49.7 | 12.2 |
| | | PGD | 61.9 | 31.4 | 30.5 |
| | | MEF | 61.9 | 31.1 | 30.8 |
| | | MI | 61.9 | 31.6 | 30.3 |
| | | MDCS-MI | 61.9 | 27.0 | 34.9 |

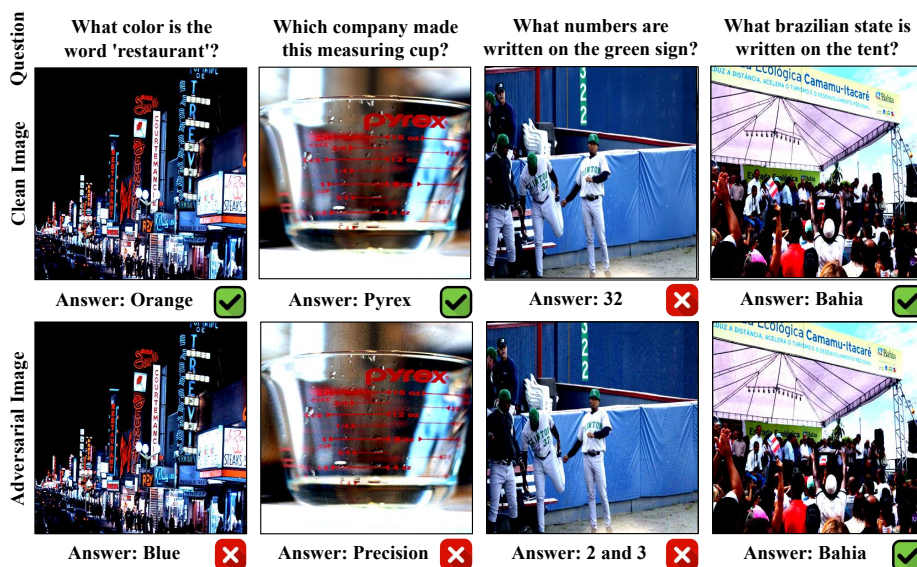


Figure 9. A comparison between responses from the clean image and the adversarial image generated by MDCS-MI against prismVLM. Image and questions source are from textVQA.

Table 7. Detailed comparison of attack success rates on Flickr30K dataset. The gray-shaded cells represent attacks in a white-box setting, while the remaining cells show results for black-box transfer attacks. We report the attack success rates (%) for cross modal retrieval tasks using R@1, R@5, and R@10 metrics. The adversarial perturbations are constrained by an L_∞ norm of $8/255$, generated over 10 iterations with a step-size of $2/255$.

| FLICKR30K (Image-Text Retrieval) | | | | | | | | | | | | | |
|----------------------------------|-------------------|--------------|--------------|--------------|--------------|--------------|--------------|---------------------|--------------|--------------|---------------------|--------------|--------------|
| Source | Attack | ALBEF | | | TCL | | | CLIP _{VIT} | | | CLIP _{CNN} | | |
| | | R@1 | R@5 | R@10 | R@1 | R@5 | R@10 | R@1 | R@5 | R@10 | R@1 | R@5 | R@10 |
| ALBEF | Co-Attack | 97.1 | 94.59 | 92.60 | 39.52 | 20.40 | 14.53 | 29.82 | 11.73 | 6.61 | 31.29 | 11.73 | 5.77 |
| | SGA | 99.79 | 99.80 | 99.80 | 87.67 | 77.09 | 70.54 | 38.04 | 19.11 | 13.11 | 41.63 | 21.56 | 14.62 |
| | MDCS-SGA | 100.0 | 100.0 | 100.0 | 91.78 | 82.11 | 76.75 | 41.35 | 22.64 | 15.55 | 45.08 | 25.90 | 17.71 |
| | DRA | 99.79 | 99.80 | 99.80 | 89.78 | 80.90 | 75.75 | 46.63 | 24.30 | 18.60 | 50.32 | 27.91 | 20.19 |
| | MDCS-DRA | 99.9 | 99.80 | 99.80 | 93.26 | 85.63 | 79.26 | 49.94 | 28.35 | 20.43 | 55.56 | 32.66 | 23.38 |
| | SA-AET | 99.9 | 99.80 | 99.80 | 96.31 | 92.56 | 89.58 | 54.23 | 33.13 | 24.90 | 58.88 | 37.53 | 27.50 |
| | MDCS-SAAET | 99.9 | 99.90 | 99.90 | 96.52 | 94.47 | 91.88 | 60.25 | 38.53 | 29.17 | 60.54 | 42.71 | 32.13 |
| TCL | Co-Attack | 49.84 | 27.45 | 60.36 | 91.68 | 85.23 | 80.96 | 32.64 | 13.40 | 6.81 | 32.06 | 14.27 | 8.14 |
| | SGA | 93.33 | 87.17 | 83.70 | 100.0 | 100.0 | 100.0 | 37.42 | 18.28 | 12.20 | 42.02 | 22.73 | 15.65 |
| | MDCS-SGA | 95.10 | 90.08 | 87.10 | 100.0 | 100.0 | 100.0 | 42.45 | 21.18 | 15.75 | 46.87 | 26.74 | 20.29 |
| | DRA | 95.31 | 91.18 | 89.80 | 100.0 | 100.0 | 99.90 | 46.26 | 26.38 | 18.50 | 50.70 | 30.66 | 21.83 |
| | MDCS-DRA | 96.66 | 92.48 | 90.70 | 100.0 | 100.0 | 100.0 | 50.92 | 28.35 | 20.83 | 56.19 | 34.88 | 25.44 |
| | SA-AET | 98.85 | 96.69 | 95.40 | 100.0 | 100.0 | 100.0 | 53.99 | 33.02 | 26.42 | 59.64 | 39.96 | 30.38 |
| | MDCS-SAAET | 99.17 | 96.69 | 96.10 | 100.0 | 100.0 | 100.0 | 57.79 | 39.25 | 29.17 | 62.71 | 44.19 | 34.29 |
| CLIP _{VIT} | Co-Attack | 8.55 | 1.50 | 0.50 | 10.01 | 2.01 | 0.70 | 78.5 | 57.4 | 45.53 | 29.50 | 11.42 | 6.08 |
| | SGA | 21.58 | 8.02 | 5.10 | 24.66 | 9.45 | 4.91 | 100.0 | 100.0 | 99.9 | 52.49 | 34.04 | 25.23 |
| | MDCS-SGA | 29.30 | 13.23 | 8.60 | 30.56 | 13.07 | 8.52 | 100.0 | 100.0 | 100.0 | 57.60 | 37.32 | 28.73 |
| | DRA | 27.95 | 11.92 | 7.90 | 29.08 | 12.56 | 7.72 | 100.0 | 99.90 | 99.80 | 62.45 | 42.81 | 31.72 |
| | MDCS-DRA | 34.41 | 15.63 | 11.40 | 35.51 | 15.08 | 9.92 | 100.0 | 100.0 | 100.0 | 68.45 | 46.51 | 37.08 |
| | SA-AET | 35.97 | 19.74 | 15.30 | 37.93 | 19.90 | 13.83 | 100.0 | 100.0 | 100.0 | 69.09 | 50.11 | 42.12 |
| | MDCS-SAAET | 42.34 | 23.35 | 18.30 | 43.52 | 25.03 | 17.84 | 100.0 | 100.0 | 100.0 | 73.18 | 55.29 | 46.34 |
| CLIP _{CNN} | Co-Attack | 10.53 | 1.60 | 0.40 | 12.54 | 2.01 | 0.70 | 27.24 | 12.05 | 6.50 | 95.91 | 89.75 | 85.99 |
| | SGA | 15.02 | 4.71 | 2.50 | 18.34 | 6.33 | 3.21 | 39.51 | 19.83 | 12.70 | 100.0 | 99.58 | 99.38 |
| | MDCS-SGA | 19.19 | 8.62 | 5.00 | 23.92 | 9.25 | 6.01 | 45.89 | 24.30 | 17.68 | 99.87 | 99.68 | 99.59 |
| | DRA | 19.08 | 6.41 | 3.30 | 22.02 | 7.14 | 3.01 | 48.34 | 26.48 | 17.99 | 100.0 | 99.58 | 99.28 |
| | MDCS-DRA | 23.04 | 10.02 | 6.40 | 25.82 | 10.45 | 6.51 | 55.83 | 31.98 | 22.15 | 100.0 | 99.68 | 99.59 |
| | SA-AET | 23.88 | 9.12 | 6.00 | 25.18 | 10.05 | 6.91 | 54.60 | 31.26 | 23.78 | 100.0 | 100.0 | 99.79 |
| | MDCS-SAAET | 30.76 | 13.93 | 10.00 | 33.40 | 15.68 | 10.52 | 61.72 | 41.33 | 31.50 | 100.0 | 100.0 | 100.0 |
| FLICKR30K (Text-Image Retrieval) | | | | | | | | | | | | | |
| Source | Attack | ALBEF | | | TCL | | | CLIP _{VIT} | | | CLIP _{CNN} | | |
| | | R@1 | R@5 | R@10 | R@1 | R@5 | R@10 | R@1 | R@5 | R@10 | R@1 | R@5 | R@10 |
| ALBEF | Co-Attack | 98.36 | 96.41 | 94.86 | 51.24 | 31.90 | 24.41 | 38.92 | 23.31 | 17.01 | 41.99 | 25.18 | 18.55 |
| | SGA | 99.95 | 99.88 | 99.88 | 87.88 | 77.07 | 70.94 | 46.17 | 28.40 | 21.96 | 50.36 | 32.24 | 24.67 |
| | MDCS-SGA | 99.98 | 99.96 | 99.96 | 91.24 | 81.87 | 75.55 | 49.71 | 30.88 | 23.68 | 53.93 | 35.15 | 27.69 |
| | DRA | 99.91 | 99.92 | 99.86 | 90.52 | 82.05 | 76.42 | 57.28 | 38.15 | 29.87 | 59.11 | 41.41 | 33.59 |
| | MDCS-DRA | 99.98 | 99.92 | 99.92 | 92.98 | 85.67 | 80.63 | 59.31 | 40.74 | 31.95 | 62.44 | 45.20 | 36.05 |
| | SA-AET | 100.0 | 99.90 | 99.90 | 96.19 | 92.21 | 89.32 | 63.50 | 45.95 | 36.81 | 65.18 | 48.37 | 39.87 |
| | MDCS-SAAET | 100.0 | 99.94 | 99.92 | 96.71 | 93.24 | 90.48 | 67.01 | 49.19 | 40.86 | 67.89 | 51.80 | 43.51 |
| TCL | Co-Attack | 60.36 | 41.59 | 33.26 | 95.48 | 90.32 | 86.74 | 42.69 | 26.44 | 20.37 | 47.82 | 30.47 | 23.13 |
| | SGA | 92.84 | 87.31 | 83.46 | 100.0 | 100.0 | 100.0 | 46.39 | 29.57 | 22.50 | 51.36 | 33.38 | 25.23 |
| | MDCS-SGA | 94.69 | 89.54 | 86.78 | 100.0 | 100.0 | 100.0 | 49.19 | 31.58 | 25.05 | 55.71 | 37.17 | 28.33 |
| | DRA | 95.35 | 91.57 | 89.04 | 100.0 | 99.98 | 99.94 | 56.80 | 39.31 | 31.62 | 61.54 | 43.57 | 35.01 |
| | MDCS-DRA | 96.42 | 92.92 | 90.96 | 100.0 | 100.0 | 100.0 | 59.76 | 41.91 | 35.02 | 65.01 | 46.89 | 38.60 |
| | SA-AET | 98.48 | 96.82 | 95.43 | 99.98 | 99.96 | 99.96 | 63.27 | 46.13 | 38.42 | 68.44 | 50.68 | 42.04 |
| | MDCS-SAAET | 98.88 | 97.13 | 96.20 | 100.0 | 100.0 | 99.98 | 65.98 | 49.71 | 42.02 | 71.01 | 54.20 | 45.92 |
| CLIP _{VIT} | Co-Attack | 20.18 | 9.54 | 7.12 | 21.29 | 9.51 | 6.78 | 87.50 | 77.95 | 73.40 | 38.49 | 23.19 | 17.87 |
| | SGA | 34.89 | 18.07 | 13.69 | 35.83 | 18.79 | 14.11 | 100.0 | 100.0 | 100.0 | 60.38 | 42.58 | 35.19 |
| | MDCS-SGA | 40.69 | 21.90 | 16.28 | 39.81 | 22.45 | 16.02 | 100.0 | 100.0 | 100.0 | 66.00 | 48.20 | 39.71 |
| | DRA | 43.29 | 24.63 | 18.82 | 44.83 | 25.76 | 19.39 | 100.0 | 100.0 | 99.96 | 69.47 | 53.88 | 45.06 |
| | MDCS-DRA | 48.15 | 28.63 | 21.69 | 48.40 | 28.65 | 22.24 | 100.0 | 100.0 | 100.0 | 73.41 | 57.79 | 49.24 |
| | SA-AET | 50.28 | 32.08 | 25.76 | 51.36 | 32.77 | 26.18 | 100.0 | 99.98 | 99.98 | 74.00 | 59.22 | 51.62 |
| | MDCS-SAAET | 54.86 | 36.89 | 29.32 | 55.45 | 36.49 | 29.16 | 100.0 | 99.98 | 99.96 | 77.53 | 63.15 | 55.61 |
| CLIP _{CNN} | Co-Attack | 23.62 | 11.40 | 8.21 | 26.05 | 12.69 | 8.79 | 40.62 | 24.71 | 18.82 | 96.50 | 92.75 | 90.35 |
| | SGA | 28.60 | 14.99 | 10.92 | 32.26 | 17.32 | 12.67 | 51.16 | 33.45 | 25.56 | 100.0 | 99.90 | 99.73 |
| | MDCS-SGA | 33.44 | 17.86 | 12.90 | 36.48 | 19.02 | 14.09 | 56.22 | 38.64 | 30.14 | 100.0 | 99.95 | 99.86 |
| | DRA | 33.96 | 18.50 | 13.49 | 37.45 | 20.74 | 15.13 | 59.02 | 40.55 | 32.75 | 99.93 | 99.59 | 99.28 |
| | MDCS-DRA | 39.43 | 22.29 | 16.60 | 41.05 | 23.53 | 17.83 | 63.89 | 45.60 | 36.89 | 100.0 | 99.93 | 99.82 |
| | SA-AET | 37.89 | 21.68 | 16.52 | 41.69 | 24.33 | 18.14 | 63.14 | 44.45 | 35.52 | 99.97 | 99.78 | 99.62 |
| | MDCS-SAAET | 45.02 | 27.71 | 21.17 | 47.57 | 30.10 | 22.68 | 69.56 | 52.18 | 43.76 | 99.97 | 99.88 | 99.82 |

Table 8. Detailed comparison of attack success rates on MSCOCO dataset. We report the attack success rates (%) for both Image-Text Retrieval and Text-Image Retrieval tasks using R@1, R@5, and R@10 metrics. The adversarial perturbations are constrained by an L_∞ norm of 8/255, generated over 10 iterations with a step size of 2/255.

| MSCOCO (Image-Text Retrieval) | | | | | | | | | | | | | |
|-------------------------------|-------------------|--------------|--------------|--------------|--------------|--------------|--------------|---------------------|--------------|--------------|---------------------|--------------|--------------|
| Source | Attack | ALBEF | | | TCL | | | CLIP _{VIT} | | | CLIP _{CNN} | | |
| | | R@1 | R@5 | R@10 | R@1 | R@5 | R@10 | R@1 | R@5 | R@10 | R@1 | R@5 | R@10 |
| ALBEF | Co-Attack | 96.65 | 94.74 | 93.12 | 57.33 | 37.24 | 28.53 | 50.71 | 33.10 | 26.44 | 52.06 | 33.89 | 27.47 |
| | SGA | 99.95 | 99.70 | 99.65 | 87.22 | 76.39 | 69.34 | 64.06 | 46.76 | 39.02 | 63.34 | 47.67 | 39.72 |
| | MDCS-SGA | 100.0 | 99.96 | 99.84 | 88.23 | 77.94 | 70.73 | 64.94 | 49.08 | 40.44 | 66.12 | 49.63 | 41.83 |
| | DRA | 99.92 | 99.68 | 99.44 | 88.78 | 78.81 | 72.24 | 69.21 | 52.56 | 43.97 | 69.06 | 52.13 | 43.87 |
| | MDCS-DRA | 100.0 | 99.85 | 99.77 | 90.29 | 80.75 | 74.00 | 71.77 | 54.26 | 45.61 | 71.19 | 55.04 | 46.49 |
| | SA-AET | 100.0 | 99.96 | 99.96 | 96.98 | 93.45 | 90.11 | 76.61 | 61.51 | 53.76 | 75.32 | 61.03 | 53.19 |
| | MDCS-SAAET | 100.0 | 99.96 | 99.94 | 97.54 | 94.03 | 91.04 | 79.28 | 65.25 | 57.33 | 78.05 | 64.16 | 56.44 |
| TCL | Co-Attack | 65.22 | 45.39 | 36.43 | 94.95 | 91.18 | 89.08 | 55.28 | 38.04 | 29.73 | 56.68 | 37.31 | 29.82 |
| | SGA | 92.78 | 86.95 | 83.68 | 100.0 | 99.98 | 99.96 | 58.68 | 44.11 | 36.70 | 61.05 | 45.91 | 38.36 |
| | MDCS-SGA | 93.50 | 88.63 | 85.36 | 100.0 | 100.0 | 100.0 | 62.15 | 46.39 | 39.56 | 62.44 | 48.68 | 40.94 |
| | DRA | 94.61 | 90.49 | 87.90 | 100.0 | 100.0 | 99.96 | 71.08 | 54.81 | 46.53 | 70.29 | 54.94 | 45.89 |
| | MDCS-DRA | 95.64 | 91.81 | 89.05 | 100.0 | 100.0 | 99.98 | 72.30 | 56.36 | 48.76 | 72.82 | 57.71 | 48.58 |
| | SA-AET | 97.96 | 95.78 | 93.95 | 100.0 | 99.98 | 99.96 | 76.00 | 61.54 | 54.63 | 75.64 | 61.00 | 53.51 |
| | MDCS-SAAET | 98.12 | 95.97 | 94.55 | 100.0 | 99.96 | 99.90 | 78.33 | 64.84 | 57.29 | 79.12 | 65.79 | 56.86 |
| CLIP _{VIT} | Co-Attack | 26.35 | 11.97 | 7.20 | 28.23 | 12.89 | 8.19 | 88.78 | 78.21 | 70.98 | 47.36 | 31.49 | 25.29 |
| | SGA | 43.88 | 25.53 | 17.99 | 43.73 | 25.44 | 18.23 | 100.0 | 100.0 | 100.0 | 71.60 | 56.46 | 48.63 |
| | MDCS-SGA | 48.47 | 28.96 | 20.96 | 47.75 | 28.29 | 20.71 | 100.0 | 100.0 | 100.0 | 74.09 | 59.94 | 52.22 |
| | DRA | 52.08 | 32.42 | 23.88 | 51.67 | 31.65 | 23.73 | 100.0 | 99.95 | 99.95 | 80.79 | 67.72 | 60.64 |
| | MDCS-DRA | 56.30 | 36.41 | 28.00 | 55.32 | 34.58 | 26.21 | 100.0 | 99.97 | 99.98 | 82.63 | 71.04 | 63.75 |
| | SA-AET | 57.90 | 38.93 | 29.81 | 57.41 | 38.14 | 30.06 | 99.96 | 99.97 | 99.93 | 84.51 | 73.48 | 66.63 |
| | MDCS-SAAET | 62.80 | 44.26 | 34.89 | 62.43 | 42.56 | 34.53 | 100.0 | 99.95 | 99.93 | 85.70 | 76.12 | 70.44 |
| CLIP _{CNN} | Co-Attack | 29.49 | 13.26 | 8.28 | 31.83 | 15.11 | 9.81 | 53.15 | 36.11 | 28.78 | 97.79 | 94.29 | 92.26 |
| | SGA | 36.58 | 19.14 | 11.90 | 38.47 | 20.38 | 14.19 | 62.69 | 47.46 | 38.64 | 99.96 | 99.84 | 99.68 |
| | MDCS-SGA | 40.53 | 21.90 | 14.64 | 43.28 | 24.11 | 17.05 | 66.58 | 52.15 | 44.23 | 99.96 | 99.97 | 99.95 |
| | DRA | 41.09 | 21.58 | 14.41 | 43.25 | 23.59 | 16.36 | 70.89 | 55.21 | 46.46 | 99.75 | 99.70 | 99.32 |
| | MDCS-DRA | 45.60 | 25.67 | 18.05 | 48.17 | 27.71 | 20.31 | 75.70 | 61.02 | 52.57 | 99.96 | 99.92 | 99.78 |
| | SA-AET | 43.57 | 24.85 | 17.35 | 47.04 | 26.65 | 19.24 | 72.61 | 57.95 | 50.20 | 99.92 | 99.84 | 99.76 |
| | MDCS-SAAET | 50.71 | 31.17 | 22.87 | 53.04 | 33.03 | 24.24 | 79.13 | 66.90 | 59.04 | 100.0 | 99.95 | 99.90 |
| MSCOCO (Text-Image Retrieval) | | | | | | | | | | | | | |
| Source | Attack | ALBEF | | | TCL | | | CLIP _{VIT} | | | CLIP _{CNN} | | |
| | | R@1 | R@5 | R@10 | R@1 | R@5 | R@10 | R@1 | R@5 | R@10 | R@1 | R@5 | R@10 |
| ALBEF | Co-Attack | 98.33 | 96.60 | 95.30 | 64.19 | 46.17 | 37.83 | 57.36 | 42.19 | 35.53 | 60.74 | 45.90 | 38.77 |
| | SGA | 99.95 | 99.81 | 99.73 | 87.96 | 76.98 | 70.35 | 70.01 | 55.43 | 48.06 | 70.95 | 56.31 | 49.00 |
| | MDCS-SGA | 99.99 | 99.95 | 99.92 | 88.28 | 77.93 | 71.47 | 70.88 | 56.85 | 49.08 | 72.08 | 57.69 | 50.76 |
| | DRA | 99.96 | 99.79 | 99.66 | 90.01 | 80.25 | 73.80 | 74.89 | 61.34 | 53.78 | 75.11 | 61.74 | 54.39 |
| | MDCS-DRA | 99.97 | 99.89 | 99.82 | 90.92 | 81.56 | 75.38 | 76.28 | 62.76 | 55.42 | 77.42 | 63.53 | 56.37 |
| | SA-AET | 99.99 | 99.96 | 99.92 | 96.87 | 93.16 | 90.34 | 79.99 | 68.16 | 61.23 | 80.86 | 68.58 | 61.39 |
| | MDCS-SAAET | 99.99 | 99.96 | 99.93 | 97.25 | 94.02 | 91.46 | 81.91 | 70.70 | 63.88 | 82.51 | 70.60 | 63.92 |
| TCL | Co-Attack | 72.41 | 56.37 | 48.16 | 97.87 | 95.32 | 93.42 | 62.33 | 46.90 | 39.68 | 66.45 | 49.95 | 42.72 |
| | SGA | 93.07 | 87.82 | 84.17 | 100.0 | 100.0 | 100.0 | 64.89 | 50.93 | 43.85 | 67.46 | 53.56 | 46.29 |
| | MDCS-SGA | 94.29 | 89.04 | 85.66 | 100.0 | 100.0 | 100.0 | 67.56 | 52.76 | 45.77 | 69.72 | 56.45 | 49.05 |
| | DRA | 95.74 | 91.87 | 89.31 | 99.99 | 99.99 | 99.98 | 75.14 | 61.13 | 53.92 | 76.87 | 63.69 | 56.22 |
| | MDCS-DRA | 96.49 | 92.67 | 90.14 | 100.0 | 99.99 | 99.99 | 76.68 | 63.53 | 56.24 | 78.68 | 65.78 | 58.75 |
| | SA-AET | 98.06 | 95.93 | 94.57 | 99.99 | 99.95 | 99.94 | 79.96 | 67.85 | 61.25 | 81.09 | 69.43 | 62.51 |
| | MDCS-SAAET | 98.17 | 96.16 | 94.94 | 99.99 | 99.97 | 99.93 | 81.55 | 70.18 | 63.87 | 83.07 | 71.90 | 65.28 |
| CLIP _{VIT} | Co-Attack | 36.69 | 22.86 | 17.71 | 38.42 | 23.51 | 17.88 | 96.72 | 91.28 | 85.46 | 58.45 | 43.78 | 36.77 |
| | SGA | 51.04 | 33.62 | 27.06 | 50.83 | 34.42 | 27.92 | 100.0 | 100.0 | 100.0 | 75.59 | 63.21 | 56.28 |
| | MDCS-SGA | 54.76 | 36.70 | 29.42 | 53.25 | 36.42 | 29.66 | 100.0 | 100.0 | 100.0 | 78.42 | 66.56 | 59.98 |
| | DRA | 61.51 | 43.47 | 36.22 | 60.81 | 43.89 | 36.16 | 100.0 | 100.0 | 99.99 | 84.61 | 74.06 | 67.92 |
| | MDCS-DRA | 64.52 | 46.76 | 38.89 | 62.95 | 46.17 | 38.31 | 100.0 | 100.0 | 99.99 | 86.00 | 77.26 | 71.28 |
| | SA-AET | 66.21 | 49.54 | 42.24 | 65.50 | 49.36 | 41.87 | 99.99 | 99.97 | 99.95 | 87.32 | 77.99 | 72.27 |
| | MDCS-SAAET | 70.09 | 53.98 | 46.53 | 68.75 | 52.97 | 45.26 | 100.0 | 99.98 | 99.98 | 89.18 | 80.13 | 74.96 |
| CLIP _{CNN} | Co-Attack | 41.50 | 26.14 | 20.51 | 43.44 | 27.92 | 21.61 | 60.15 | 45.53 | 38.56 | 98.54 | 96.16 | 94.71 |
| | SGA | 46.29 | 30.00 | 23.70 | 48.75 | 32.86 | 26.01 | 67.89 | 53.23 | 46.93 | 99.95 | 99.85 | 99.76 |
| | MDCS-SGA | 50.04 | 32.89 | 26.19 | 51.72 | 35.26 | 27.89 | 72.24 | 58.48 | 51.84 | 99.97 | 99.96 | 99.94 |
| | DRA | 52.32 | 35.71 | 28.85 | 54.26 | 37.89 | 30.60 | 74.83 | 62.53 | 55.45 | 99.93 | 99.76 | 99.64 |
| | MDCS-DRA | 56.64 | 39.42 | 32.21 | 57.84 | 41.30 | 33.90 | 78.85 | 66.94 | 60.37 | 99.97 | 99.91 | 99.84 |
| | SA-AET | 54.86 | 38.13 | 31.21 | 57.84 | 40.16 | 32.96 | 76.95 | 64.59 | 57.86 | 99.91 | 99.81 | 99.65 |
| | MDCS-SAAET | 60.76 | 44.01 | 36.78 | 62.13 | 45.37 | 37.92 | 82.75 | 71.77 | 65.13 | 99.97 | 99.91 | 99.80 |